TWO-DIMENSIONAL CRYSTALLIZATION OF ARCHAEAL SIGNAL PEPTIDE PEPTIDASES FOR STRUCTURAL STUDIES BY ELECTRON CRYSTALLOGRAPHY

A Thesis
Presented to
The Academic Faculty

by

Maureen Grage Metcalfe

In Partial Fulfillment
of the Requirements for the Degree
Master of Science in the
School of Biology

Georgia Institute of Technology
August 2014

TWO-DIMENSIONAL CRYSTALLIZATION OF ARCHAEAL SIGNAL PEPTIDE PEPTIDASES FOR STRUCTURAL STUDIES BY ELECTRON CRYSTALLOGRAPHY

Approved by:

Dr. Ingeborg Schmidt-Krey, Advisor
School of Biology
School of Chemistry and Biochemistry
Georgia Institute of Technology

Dr. Raquel Lieberman
School of Biochemistry
Georgia Institute of Technology

Dr. Nael A. McCarty
School of Biology
Georgia Institute of Technology
Department of Pediatrics
Emory University

Date Approved: March 13, 2014

This accumulation of letters, numbers and images is dedicated to the many people who kept me smiling and laughing.

ACKNOWLEDGEMENTS

I would like to thank Ingeborg Schmidt-Krey, PhD, my ever so patient advisor and friend for mentoring and encouraging me for the past four years on this project. Thank you to my committee, Raquel Lieberman, PhD and Nael McCarty, PhD. This wasn't a typical master's research project or timeline. Thank you for sticking with me on this project and providing meaningful advice and support. I would like to thank current and past members from Schmidt-Krey's laboratory as well as Raquel Lieberman's laboratory. A special thank you to Matthew Johnson, PhD, Yusuf Uddin, Kerry McGill, Laura Kim, and Sibel Kalyoncu for all their help.

None of this would have happened if I didn't have support outside of Georgia Tech. To that point, I would have never met Inga if it hadn't been for my laboratory dad, Charles Humphrey, PhD. I couldn't have completed any of this without your support and understanding. I know that this took a while to complete. Thank you a million times over for working with me and my crazy schedule. I would also like to express a sincere thanks to the laboratory members I work with on a daily basis outside of Georgia Tech: Amy D, Amy S, Atis, Brigid, Charles, Chris, Clifton, Cynthia G, Cynthia S, Dianna (+Aeb and Early), Dominique, Heather, Jana, Jeanine, Jeltley, Julu, Libby, Lindy, Marlene, Mitesh, Pat, Ray, Renae, Sherry, Sherif, Shieh, and Tara. Thank you for being my second family.

Back in Washington State, I would like to thank my family, mommy, daddy, Marit (plus Marit's partner, Stori), and Spencer. My family bore the brunt of my frustrations. One week it would be a call home announcing I was a total failure only to be followed weeks later with amazing news that the experiment worked – I was a genius!! If they would have asked if I was bipolar, I probably would have said yes and so were my

proteins that I worked with in lab. Thank you for always listening. Sometimes I just needed to hear a familiar voice to know I wasn't by myself walking out to the parking lot in the middle of the night. Thank you for the constant supportive phone calls. I am sorry I don't always pick up but the fact that you called to check in means so much.

Electron microscopy would have never been a passion, let alone a career path, if it hadn't been for Valarie Lynch-Holmes and Christine Davitt at Washington State University in Pullman, WA. I can't imagine my life without an electron microscope and the small world located on a 3 mm grid that I get to look at and experience everyday because of both of them.

To all my west coast friends and second sets of parents, Alan Quon (for realizing when I need rescuing and a long vacation), Megan Lee (my second sister who is always there when times get tough and ready to raise a glass to celebrate when goals are accomplished), Mallory Day, Megan Taft, Danny Lauer, Emily Messmer, Melanie Deguise, Britni Freiboth, Dustin Hansen, Stephanie Pitts, Nick Rodgers, and Ian Stewart. To my additional parents: Bob and Rhonna Lee, Denny and Cindy Brune; that have been so supportive of my efforts to continue learning and constant reminders to enjoy life. Thank you so much for you support and conversations.

Karma would come back to bite me if I didn't mention the amazing people I have met in Atlanta, Samantha Lasater, MS, Taylor Updegrove, PhD, Larisa Pender-Healy, PhD, Kari Fine, DVM, PhD, Susan Orwig, PhD and Jason Drury, PhD. My sanity would have never stayed intact, my stomach would have been empty more times than full, and laughter would have never filled the air without this irreplaceable group of people. Special thank you to Samantha for late night dessert runs to Cafe Intermezzo and La

Tavola (Molto Mondays and Alli Royce), which served as some of the best therapy sessions I happily paid for. Thank you to Jason for working late, providing countless purifications, runs in the park and amazing games of frisbee. I would have never gotten this far and achieved the results I have obtained without your efforts from the very beginning. They provided a solid foundation that culminated into the efforts and results reported within this body of work. To Kari Fine for supportive and motivating conversations. To Taylor for motivating and inspiring me to keep going - keep riding the wave of good results! My last year at Tech would have never been the same if wasn't for Larisa (and Lucifer) – thank you so much for all the fun late nights of dancing, eating and random stuff your brought into the office. Thank you all for making life easier and more delicious.

TABLE OF CONTENTS

LIST OF TABLES

LIST OF FIGURES

LIST OF SYMBOLS AND ABBREVIATIONS

2D	two-dimensional
3D	three-dimensional
Å	Ångstrom
ASP	ammonium sulfate precipitation
CCD	charge coupled device
CMC	critical micelle concentration
cryo-EM	electron cryo-microscopy
DDM	n-Dodecyl-β-D-Maltopyranoside
DMPC	dimyristoyl phosphatidyl choline
ER	endoplasmic reticulum
FC12	fos-choline 12
FFT	fast Fourier transform
HEPES	4-(2-hydroxyethyl)-1-piperazineethanesulfonic acid
I-CLiPs	intramembrane cleaving proteases
LPR	lipid-to-protein ratio
MCMJRSPP	*Methanoculleus marisnigri* JR1 SPP
MES	2-(N-morpholino) ethanesulfonic acid
$MgCl_2$	magnesium chloride
mSPP	*Haloarcula morismortui* SPP
MWCO	molecular weight cut-off
NaCl	sodium chloride
Na-DOC	sodium deoxycholate
NaN_3	sodium azide

PAL	proline-alanine-leucine
PDB	Protein Data Bank
PS	presenilin
SPP	signal peptide peptidase
SPPL	signal peptide peptidase like

SUMMARY

The membrane proteins signal peptide peptidase, signal peptide peptidase like and presenilin are intramembrane aspartyl proteases located in the endoplasmic reticulum, plasma membrane and organelles. These membrane proteins are able to catalyze a hydrolytic reaction in a hydrophobic space. The downstream consequences of these reactions impact a variety of cellular functions such as cytokine production, inflammatory responses, embryogenesis, and immune system regulation. Additionally, the aspartyl proteases such as signal peptide peptidase and presenilin, a part of the γ-secretase complex, hydrolyze peptides leading to pathogen maturation and Alzheimer's disease, respectively.

Electron crystallography offers the unique aspect of studying membrane proteins in a near native state. Determining the structures of *Haloarcula morismortui* and *Methanoculleus marisnigri* JR1 signal peptide peptidases by electron crystallography may provide insight into how a hydrolysis reaction occurs in a hydrophobic environment and how the protein determines which transmembrane signal peptides to cleave. Additionally, structure determination may help answer questions regarding why human presenilin, part of the γ-secretase complex, incorrectly processes amyloid precursor protein into amyloid-beta peptides leading to Alzheimer's disease. Such structural data may not only shed light on how amyloid precursor protein is processed but how other proteins are processed by signal peptide peptidase leading to immune responses, cell signaling, and pathogen maturation. In addition, structure-function data may have an

impact on pharmaceutical drug designs that targets signal peptide peptidase, signal peptide peptidase like, and/or presenilin.

To determine the structure of aspartyl proteases, two archaeal signal peptide peptidases were used for two-dimensional crystallization trials to be able to study their structure by electron crystallography. *Haloarcula morismortui* and *Methanoculleus marisnigri* JR1 signal peptide peptidases, both human signal peptide peptidase homologues, were recombinantly over-expressed and purified. During dialysis trials, various lipid-to-protein ratios, sodium chloride concentrations, temperatures, detergents and a variety of other variables were tested.

Methanoculleus marisnigri JR1 signal peptide peptidase showed the most promising results in terms of crystallinity. Optimizing dialysis conditions, specifically narrowing the lipid-to-protein ratio, resulted in two-dimensional crystals. Ordered arrays measuring up to 200 nm x 200 nm were observed. These ordered arrays have been shown to be reproducible amongst multiple batches of purified *Methanoculleus marisnigri* JR1 signal peptide peptidase. Preliminary projection maps of negatively stained ordered arrays show unit cell dimensions of a = 178 Å, b = 160 Å, γ = 92.0 Å and a = 175 Å, b = 167 Å, γ = 92.0 Å. The monomer measurements are approximately 70 Å by 80 Å. This is the first time a signal peptide peptidase homologue has been crystallized by two-dimensional crystallization.

CHAPTER 1

INTRODUCTION

1.1 Membrane Protein Overview

The human genome is estimated to contain 20-30% membrane proteins (1). They are found at the cell surface associated with the cellular membrane, and intracellularly, embedded within the lipid bilayers of organelles. Membrane proteins carry out a diverse set of cellular functions such as transport, enzymatic activity, signal transduction, intracellular junctions, cell-cell recognition and attachment to the cytoskeleton and extracellular matrix (2).

Membrane proteins are significant in that approximately 60% of drugs approved by the Food and Drug Administration target these types of proteins (3). In a 50 billion dollar industry three of the top four drug targets are membrane proteins and consist of the class I G-protein coupled receptors, ligand-gated ion channels and voltage-gated ion channels (4). Given these statistics, little is known about the overall structure of membrane proteins in their native membrane-bound state and the drug interactions that affect them.

There are two types of membrane proteins, those with β-barrels and those with α-helical transmembrane domains. β-barrels are composed of 8 to 24 β-sheets that form a pore. They are found in the outer membranes of Gram-negative bacteria, chloroplasts and mitochondria. They function as porins, transporters, and receptors (5). Membrane proteins with α-helical transmembrane domains are composed of one or more α-helices extending through the lipid bilayer. An α-helix is composed of a linear sequence of amino acids that fold into right-handed helices stabilized by internal hydrogen bonding. This

group of membrane proteins is critical in transport, signaling, enzymatic activity and attachment to the extracellular matrix (6).

1.2 Electron Crystallography

Henderson and Unwin solved the first three-dimensional (3D) model of the membrane protein bacteriorhodopsin at 7 Å resolution in 1975 utilizing electron crystallography (7). Since 1975, the structures of bacteriorhodopsin as well as other membrane proteins have been solved at atomic resolution (8). Approximately 0.5% of all of the structures that have been deposited into the Protein Data Bank (PDB) are membrane proteins (9). As of March 2014, out of 91246 protein entries entered in the PDB, approximately 1% are membrane proteins. The PDB currently contains 2,274 membrane protein structures as of March 2014; this number is directly related to difficulties in attempting to crystallize membrane proteins. In the case of bacteriorhodopsin, this membrane protein naturally forms two-dimensional (2D) crystalline arrays in the membrane of *Halobacterium salinarium* (10). From these naturally occurring 2D crystals, Henderson and Unwin were able to solve the first 3D structure where α-helices could be ascertained (7). Most other membrane proteins require additional steps and considerations for 2D crystallization as described and outlined in Figure 1 to achieve a 3D structure of a membrane protein.

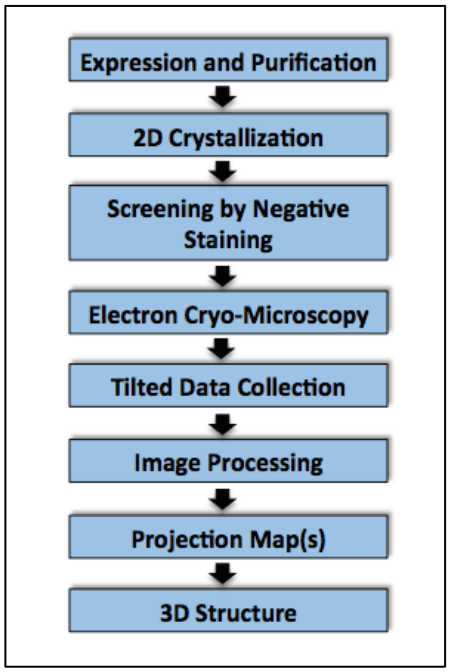

Figure 1: Overview of electron crystallography. The first step is to overexpress and purify a stable membrane protein at high concentrations for dialysis trials. Step 2 is the process of setting up 2D crystallization conditions that will lead to formation of 2D crystals. Step 3 involves negative staining and evaluating dialysis samples at the transmission electron microscope. Steps 1-3 may need to be repeated multiple times before ideal conditions are identified. Once ideal conditions are found, samples can be prepared for electron cryo-microscopy (cryo-EM) conditions. Step 4, carbon coated grids containing samples are plunged into liquid nitrogen and are kept under cryo-EM conditions. Step 5 is the process of collecting tilted images of the sample followed by image processing (step 6) and evaluation of collected data. Step 7, 2D and 3D data results in projection maps and 3D models (11).

The first hurdle is identifying an expression vector that produces adequate amounts of stable and properly folded membrane proteins that can be purified (12, 13). The step following protein purification is one of the major bottlenecks in electron crystallography 2D crystallization trials. These trials involve testing and screening many variables that may or may not produce ideal 2D crystals (14, 15, 16) Following the determination of the appropriate crystallizations parameters, the 2D crystals need to be prepared and imaged under electron cryo-microscopy (cryo-EM) conditions (17). The next step is to obtain

high resolution images (18). A stable, properly aligned transmission electron microscope with a strong coherent beam is essential for accomplishing this step. After collecting the high resolution images, image processing is necessary to generate projection maps and 3D models (19). The final outcome is a structure that may be used to describe protein function, protein-protein interactions and/or protein-drug interactions.

1.3 Intramembrane-Cleaving Proteases

Three families of intramembrane-cleaving proteases (I-CLiPs) have been identified, rhomboid, site-2, and GxGD proteases. These specialized enzymes catalyze peptide bond cleavage within the hydrophobic environment of the lipid bilayer. The I-CLiPs are involved in a range of cellular activities, which include development, organelle shaping, metabolism, pathogenicity and degenerative disease (20).

1.4 Aspartyl Proteases

Signal peptide peptidase (SPP) and homologous SPP-like (SPPL) are GxGD proteases characterized by two aspartic acid residues which activate a water molecule to cleave a peptide bond (Figure 2). These highly conserved intramembrane proteases have been found embedded in the membranes of organelles and the plasma membrane (20).

SPP/SPPL are found in a wide range of plants and organisms and contribute to a diverse set of cellular functions (21, 22, 23). SPP/SPPL are predicted to have nine transmembrane domains (24). The two catalytic aspartic acid residues characterized by YD and GxGD amino acid motifs are located on transmembrane domains 6 and 7, respectively. Another conserved motif, the proline-alanine-leucine (PAL) sequence is located on the N-terminal portion of transmembrane domain 9 (Figure 3). If proline,

alanine or leucine are mutated, SPP and PS catalytic activity is significantly diminished. (21, 22, 23, 25, 26, 27, 28)

Located in the ER, SPP cleaves signal peptides from the ER membrane after they have been released from nascent polypeptides by signal peptidase (Figure 4) (29). There is evidence that suggests that SPP exists *in vivo* as an active homodimer (30) however *in vitro* investigations utilizing x-ray crystallography and single particle analysis suggest SPP may form a homotetramer (31, 32).

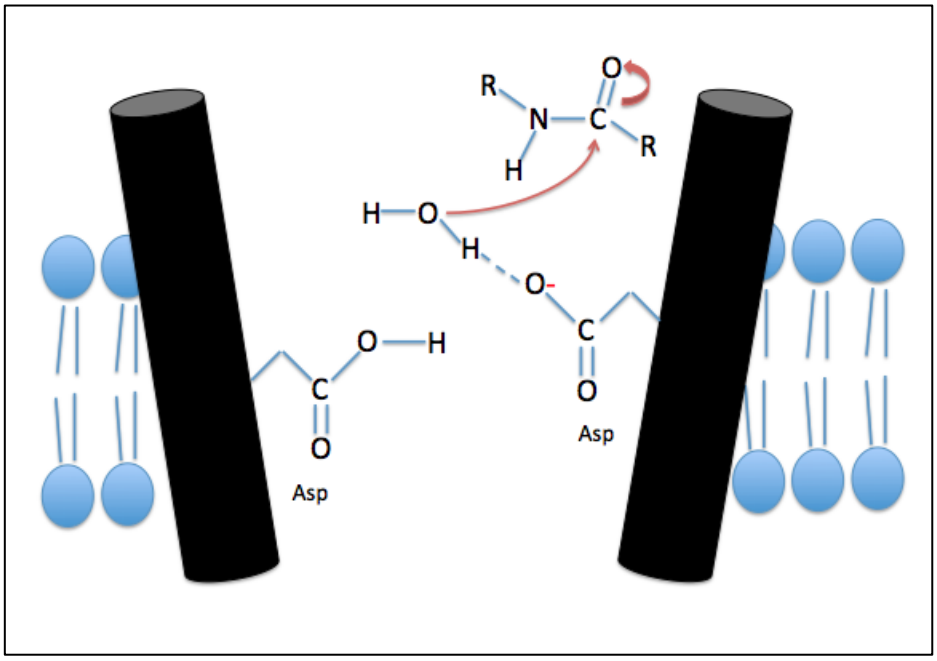

Figure 2: Proposed aspartyl protease mechanism. The two aspartate residues act like an acid-base mechanism. A water molecule situated between the two aspartate residues is activated leading to the nucleophilic oxygen molecule attacking the carbonyl group of the substrate and thus cleaving the peptide bond (20).

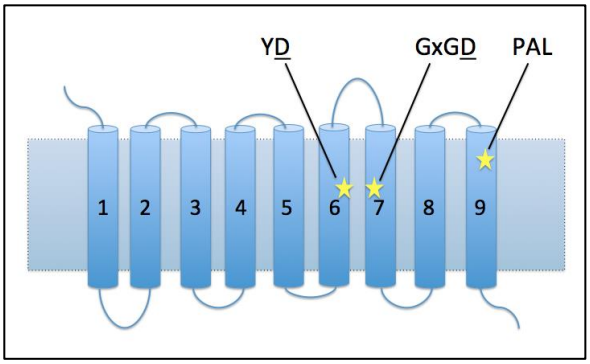

Figure 3: SPP topology. SPP contains 9 transmembrane domains with the aspartic acid residues located on transmembrane domains 6 and 7 and the PAL sequence on transmembrane domain 9 (33).

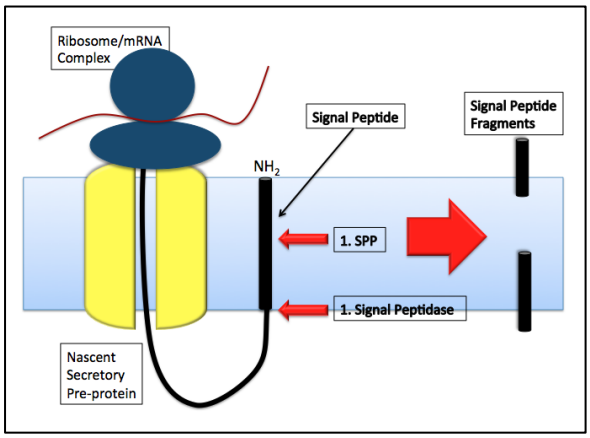

Figure 4: SPP cleavage of signal peptides from the ER membrane. Signal peptidases cleave the N-terminal signal peptide from the nascent polypeptide translating through the translocon, SPP cleaves the signal peptide releasing the fragments from the ER membrane (33).

SPP is involved in virus maturation, cellular signaling and immune surveillance. The core protein of hepatitis C virus is processed by SPP allowing for maturation of the virus (34, 35, 36). SPP is also required for the maturation of GB virus B core protein (37). SPP may be involved in the degradation of misfolded proteins (38, 39). Furthermore, SPP cleaves the signal peptide derived from newly synthesized major histocompatibility complex

class 1b molecules. This fragment is expressed as the human lymphocyte antigen binding epitope (40). Additionally, SPP cleaves the signal peptide of pre-prolactin as well as the signal peptide of HIV envelope protein p-gp160. Both peptides bind to calmodulin *in vitro*. Further investigations into the relevance of calmodulin interactions with signal peptides remains to be completed (41, 42).

Another intramembrane aspartyl protease, presenilin (PS), also is characterized by nine transmembrane domains, which contain the YD, GxGD, and PAL motifs (43). Unlike SPP, PS undergoes autoendolysis and requires additional proteins that include nicastrin, aneroid pharynx defective 1 and presenilin enhancer 2, to form the fully active γ-secretase complex. Unlike SPP/SPPL, PS transmembrane domains 6 and 7 are in the opposite orientation, enabling processing of type-I anchored membrane proteins (Figure 5) (21, 24, 44).

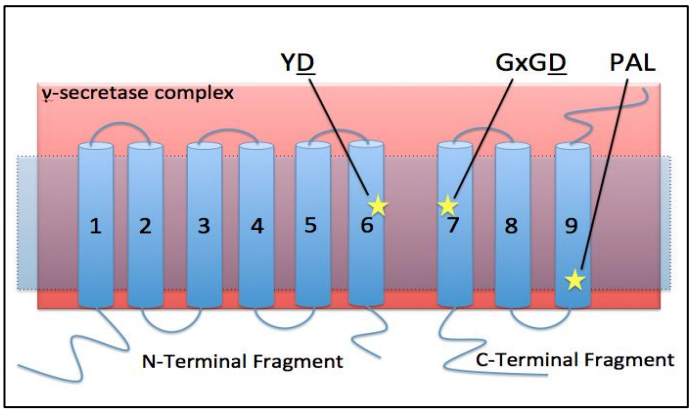

Figure 5: PS topology. PS and SPP show similar membrane topology. Presenilin contains 9 transmembrane domains and has the opposite orientation compared to SPP, allowing for processing of type I anchored membrane proteins. The aspartic acid residues are located on transmembrane domains 6 and 7 and the PAL sequence is located on transmembrane domain 9. PS undergoes post-translational processing between transmembrane domains 6 and 7. The autoendolytic activity separates PS into an N-terminal and C-terminal fragment. Additional proteins are required for PS to function and to form the ɣ-secretase complex (32).

1.5 Structural Studies of Archaeal Proteases mSPP and MCMJRSPP

To investigate the structures of aspartyl proteases SPP and PS by electron crystallography, two SPP homologues from two different archaeal bacteria were over-expressed and purified for 2D crystallization trials, *Haloarcula morismortui* SPP (mSPP) and *Methanoculleus marisnigri* JR1 (MCMJRSPP) (32) with calculated molecular weights of 36.91 kDa and 33.37 kDa, respectively.

Electron crystallography is a well-suited method for answering structure-function questions such as how aspartyl proteases like SPP and PS function in the lipid bilayer. Structural data may provide critical insights into how a hydrolysis reaction occurs in a hydrophobic environment, how SPP determines which transmembrane domains to cleave, how drugs work to inhibit SPP function, and why SPP does not cleave all transmembranes domains that are encountered.

CHAPTER 2

MATERIALS AND METHODS

2.1 Phospholipid Preparation

Lipid was prepared as previously described by Schmidt-Krey, 2007a (14). Briefly, a 10 ml ampule containing dimyristoyl phosphatidycholine (DMPC) (Avanti®) in chloroform was pipetted into a clean round-bottom flask. A steady stream of nitrogen gas was used to evaporate the chloroform. The dried DMPC was resolublized with 3.5% sodium deoxycholate (Na-DOC). The solution was placed in a sonicator for five minutes or until the DMPC was completely dissolved. After sonication, the solution was aliquoted and stored at -20ºC until use.

2.2 Lipid-to-Protein Ratio Determination

The formula below was used to calculate the lipid-to-protein ratio (LPR) in a mol:mol ratio:

$$LPR = [(C_{lipid} * V_{lipid}) / MW_{lipid}] \div [(C_{protein} * V_{protein}) / MW_{protein}] \quad \text{(Equation 1)}$$

where C_{lipid} is the concentration of DMPC, V_{lipid} is the volume of lipid, MW_{lipid} is the molecular weight of lipid (Daltons), $C_{protein}$ is the concentration of DMPC, $V_{protein}$ is the volume of protein and $MW_{protein}$ is the molecular weight of protein (Daltons).

An example of a LPR (mol/mol) calculation can be seen below for a dialysis setup using 75 µL of MCMJRSPP (33,370 Daltons), purified to 0.5 mg/mL, using 10 mg/mL DMPC, and solving to a final LPR of 18:

LPR 18 = [(10 mg/ml * V_{lipid}) / 678.15 Da] ÷ [(0.5 mg/ml * 75 µL) / 33,370 Da] = 1.371 µl V_{lipid}

2.3 Dialysis Set Up

All glassware and dialysis clips (Spectrum Laboratories, INC) were washed with a 10% aqueous solution of Extran® MA01 Concentrate and rinsed with Millipore water prior to use. Eight to ten centimeter lengths of dialysis tubing (Spectrum Laboratories, INC) with a molecular weight cut-off of 12-14000 Daltons were hydrated in Millipore water for at least 15 minutes prior to use. Aliquots of protein, previously stored at -80ºC, were kept on ice during the experiment. Aliquots of DMPC lipid were allowed to thaw at room temperature. All dialysis trials used freshly prepared detergent-free dialysis buffer. Three buffers were used during crystallization trials of mSPP and MCMJRSPP; 50 mM HEPES [pH 7.5], 10 mM NaCl, 20% glycerol (buffer 1), 20 mM HEPES [pH 7.5], 100 mM NaCl, 5 mM $MgCl_2$, 5 mM NaN_3, 20% glycerol (buffer 2), and 20 mM MES [pH 6.0], 100 mM NaCl, 5 mM $MgCl_2$, 5 mM NaN_3, 20% glycerol (buffer 3). The pH was adjusted using 5 N sodium hydroxide for all three dialysis buffers and was monitored with a pH meter (PHM250 Ion Analyzer, MeterLab®). The dialysis buffer (300 ml) was dispensed into 400 ml beakers. Next, 75 µl or 100 µl of mSPP or MCMJRSPP (overexpressed and purified in Dr. Raquel Lieberman's laboratory by Dr. Jason Drury and Sibel Kalyoncu) was mixed on ice with varying amounts of lipid depending on the desired LPR (see LPR determination). The protein-lipid mix was gently vortexed and placed immediately back on ice. The dialysis tubing was rinsed with and placed into a fresh volume of Millipore water. After 10 minutes on ice, the dialysate was once more vortexed and aliquoted into dialysis tubing that was clipped at one end. A final dialysis clip was secured prior to

submerging in dialysis buffer. The beakers were covered with aluminum foil and placed in an incubator at 24ºC for 7-12 days without any stirring or dialysis buffer exchanges.

2.4 Grid Preparation

Mica was carbon-coated and grids were subsequently prepared as previously described (49). Briefly, freshly cleaved mica was placed in a carbon evaporator (Cressington Carbon Coater 208) and sharpened and flattened carbon rods were set in place. The evaporator was allowed to reach a vacuum of 10^{-5} atm prior to initializing manual carbon coating. After carbon coating was complete, the carbon-coated mica was placed in a desiccator until use. To carbon coat grids, grids (400 mesh nickel grids, SPI® Supplies) were submerged and arranged under water on a piece of Whatman filter paper. The carbon was floated onto the water from the mica and situated over the arranged grids. The water level was gradually decreased until the carbon was completely flat over the grids. The filter paper with the carbon-coated grids was then allowed to dry in the desiccator overnight prior to use.

2.5 Negative Stain

Negative staining was performed as previously described by Schmidt-Krey, 2007a (14). Grids were held in place with non-capillary tweezers (Dumont) as 2-2.5 µl of dialysate was pipetted onto each grid and allowed to incubate for two minutes. Each grid was gently blotted from the side with Whatman filter paper and immediately stained with 2 µl of 1% uranyl acetate (aqueous). The stain was blotted after 20-30 seconds. Grids were allowed to air dry prior to examination at the TEM (JEOL 1400).

2.6 Screening

Screening negatively stained dialysis samples at the JEOL 1400 was performed as previously described (20). Briefly, the TEM was aligned prior to visualizing specimens. Samples were viewed initially at low magnifications (5-10kx). Promising coordinates within the grid plane were saved for further evaluation at intermediate magnifications (10-40kx). Intermediate magnification images were routinely captured with an Orius charge coupled device (CCD) Gatan side mount camera. Higher magnification images (50kx) were captured with an Ultrascan CCD camera. Images were evaluated using the Digital Micrograph (Gatan) software. Fast Fourier transforms (FFT) were used to assess the crystallinity of the membranes.

CHAPTER 3

TWO-DIMENSIONAL CRYSTALLIZATON OF SIGNAL PEPTIDE PEPTIDASE HOMOLOGUE FROM *Haloarcula morismortui* (mSPP)

3.1. Two-dimensional crystallization trials of ammonium sulfate precipitation cut mSPP

Protein purifications of 55-75% ammonium sulfate precipitation (ASP) cut mSPP were dialyzed against buffer 1 containing various NaCl concentrations between 10 to 100 mM and LPRs ranging from 10 to 40 (mol/mol) in dialysis experiments 9-14 (Table 1). Dialysis incubation was 7 to 9 days. Dialysis timing was considered partially based on the critical micelle concentration (CMC) of fos-choline (FC12) (1.5 mM) and previous dialysis trials (14). The starting concentration of FC12 is 0.1% w/v however, the final concentration of FC12 is unknown, due to concentrating mSPP in the final step with a 10 kDa molecular weight cut-off (MWCO) amicon filter which is known to concentrate not only the protein but FC12 as well (46).

It was observed that vesicles increased in size as NaCl concentrations decreased. At 10 mM NaCl and LPR = 10 (Table 1: D14-3) (Figure 6a), vesicles were observed and evaluated with an FFT; strong reflections were observed (Figures 6b-e). Further dialysis experiments, with the same mSPP protein batch and additional purification batches, did not show reproducible results. Based on these limited results, it was determined that mSPP can be reconstituted as well as 2D crystallized into 50 nm x 50 nm ordered arrays.

3.2 Two-dimensional crystallization trials of non-ammonium sulfate precipitation cut mSPP

Non-ASP cut mSPP was dialyzed against buffer 2 conditions for 9 days and reconstituted in a lipid bilayer (Table 1, Figure 7). Membrane vesicles and sheets were observed. The best results were observed at LPR = 40, in which case FFTs showed strong reflections (Figures 7b and c). Thus mSPP can be crystallized into a lipid bilayer producing 50 nm x 50 nm areas of 2D crystals under different buffer conditions and two LPRs, which may or may not be buffer-specific.

3.3 Co-purified lipid in non-ammonium sulfate precipitations and ammonium sulfate precipitation cuts at LPR = 0

Prior to dialysis 14, protein purification for 55-75% and 75-95% ASP cut and non-ASP cut batches of mSPP were inconsistently dialyzed at LPR = 0 to determine the presence of co-purified lipid. Early experiments that showed co-purified lipid were used for further dialysis experiments. However due to difficulties in reproducing results observed in dialysis 14-3, newly purified batches of ASP cut and non-ASP cut mSPP were dialyzed at LPR = 0 to determine the presence or absence of co-purified lipid (Figures 8a and b). Protein purification batches that showed co-purified lipid were not used for future dialysis experiments. Dialyzing protein at LPR = 0 was completed to find a consistent result where protein precipitated.

3.4 Testing of reconstitution and two-dimensional crystallization parameters

Protein concentrations between 0.1-1.0 mg/ml were tested and showed no differences following dialysis. Various mSPP purifications were used in 2D crystallization trials,

these included 0-55%, 55-75% and 75-95% ASP cuts, and concentrated and unconcentrated mSPP purifications. There were no remarkable patterns noted when various ASP cut fractions were dialyzed. Protein that was concentrated using different MWCO concentrators, such as 10 kDa, 30 kDa, and 100 kDa, did not show any significant differences. No differences were noted based on whether or not the protein was freshly purified or previously frozen and subsequently thawed for dialysis. A temperature change from 24°C to 28°C during dialysis incubation did not produce remarkably different results. Different detergents and detergent concentrations did not produce significant results. A summary of conditions tested and best conditions identified can be found in Table 2.

3.5 Discussion

The LPR appears to be important in the 2D crystallization of mSPP. Lower LPRs increase membrane crystallinity (Table 1 and 2), but needed adjustment between batches. Due to the limited success with mSPP, it cannot be concluded whether crystallization occurs entirely in an LPR-dependent manner.

Buffers 1 and 2 were found to produce good membrane morphology and sizes when tested on 55-75% ASP and non-ASP cut mSPP, respectively. Weak to strong reflections were observed in selected vesicles (Figures 6 and 7). Previously, mSPP was crystallized with buffer 1. The combination of a decrease in HEPES concentration, increase in NaCl and/or additional buffer component, magnesium chloride ($MgCl_2$), may have contributed to improved membrane morphology and crystal formation.

The vesicles that were slightly tubular showed the best reflections for mSPP for dialysis conditions 14-3 (Figure 6). For dialysis 68-2 (Figure 7), there were electron dense aggregates and vesicles. These vesicles showed weak to strong reflections.

In crystallization trials of mSPP, two detergents were utilized, FC12 and Triton-X-100 (CMC 0.10-0.16% w/v). FC12 was the solubilizing detergent that worked most successfully. However during the course of the crystallization trials of mSPP, Triton-X-100 was used. The use of Triton-X-100 did not result in mSPP reconstitution or 2D crystallization

During the crystallization trials, variations in the FC12 concentration were tested from 0.1% to 2.0%. The percentage of FC12 increases when a 10 kDa MWCO is used to concentrate FC12 solubilized protein (46). This may or may not have contributed to inconsistencies amongst batches of mSPP. None of the conditions where FC12 was varied resulted in mSPP reconstitution or 2D crystallization.

In addition to variations in protein concentrations, various ASP cuts were tested in crystallization trials for mSPP. Ammonium sulfate precipitation changes the solubility of the protein in solution. As the percentage of ammonium sulfate is increased protein precipitates. Collected fractions are designated according to the percent of ammonium sulfate used to precipitate protein. In the case of mSPP, various cuts were collected between 0-55%, 55-75% and 75-95% as well as non-ASP cut mSPP to determine if different cuts would crystallize more readily than others.

Amongst the ASP cuts and non-ASP cut, inconsistent results were observed when protein was dialyzed at LPR = 0. Two different purifications using the same ASP cut would result in precipitated protein and co-purified lipid after dialysis. The inconsistencies observed with mSPP made it impossible to determine which combination of variables contributed to the results observed in dialysis 14-3 and 68-2 (Figures 6 and 7).

There is not enough data to conclude whether co-purified lipid played a negative or positive role in the crystallization of mSPP. Further investigations with new batches of purified protein and buffer conditions may shed light on how co-purified lipid contributes or does not contribute to mSPP crystallization.

Table 1. 2D crystallization parameters for different purification batches of mSPP.

Dialysis	ASP cut & Purif. date	LPR (mol/ mol)	Buffer Conditions	Dialysis Time (days)	Results	LPR = 0 Results
D9-1	55-75% ASP Cut 06.03.10	15	Buffer 1 (25 mM NaCl)	7	Membrane structures. Weak reflections.	Co-Purified Lipid
D9-3	55-75% ASP Cut 06.03.10	15	Buffer 1 (75 mM NaCl)	7	Sheet, less than 1 μm. Weak reflections.	Co-Purified Lipid
D11-1	55-75% ASP Cut 06.03.10	15	Buffer 1 (10 mM NaCl)	7	Vesicles, less than 200 nm. Weak reflections.	Co-Purified Lipid
D12-4	55-75% ASP Cut 06.03.10	15	Buffer 1 (75 mM NaCl)	7	Vesicles, less than 1 μm. Weak reflections.	Co-Purified Lipid
D14-3	55-75% ASP Cut 06.03.10	10	Buffer 1 (10 mM NaCl)	7	Vesicles, tubes, sheets, less than 50 nm to microns. Weak reflections. Figure 6	Co-Purified Lipid
D68-2	Non-ASP cut 06.08.2010	40	Buffer 2 (100mM NaCl)	9	Vesicles and sheets, less than 50 nm to microns. Weak reflections. Figure 7	Co-Purified Lipid

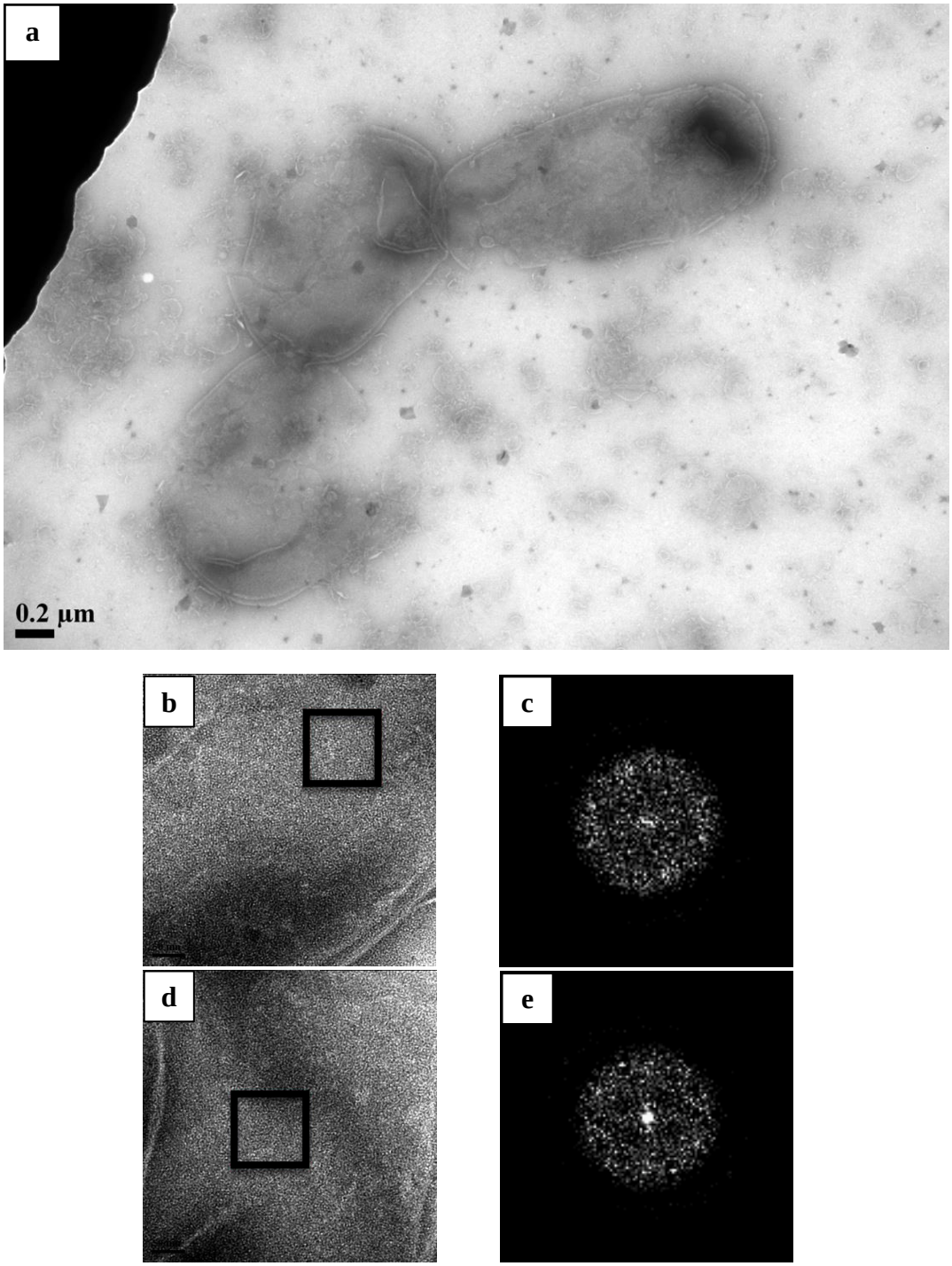

Figure 6. mSPP crystallization trials dialysis 14-3. a) Dialysis 14-3 at LPR = 10 produced vesicles. Scale bar corresponds to 0.2 µm. b-e) Higher magnifications of vesicles. The boxed areas in the high magnification images (b and d) correspond to the FFTs (c and e). Scale bar corresponds to 50 nm. FFTs revealed weak pairs of reflections indicating areas of crystallinity.

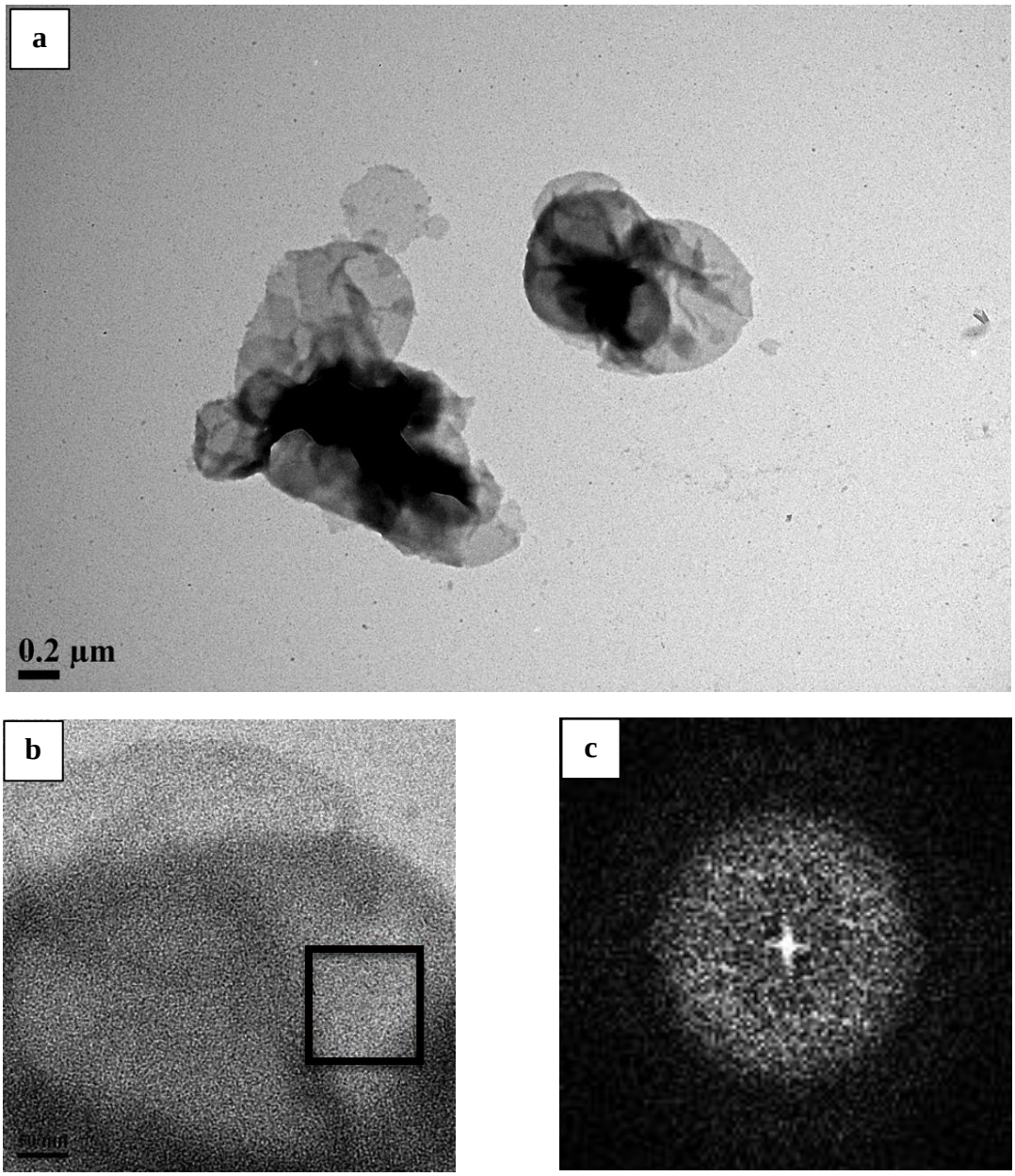

Figure 7. mSPP crystallization trials dialysis 68-2. a) Dialysis 68-2 at LPR = 40 produced vesicles. Scale bar corresponds to 0.2 µm b and c) High magnification of vesicles and associated FFT. The boxed area in the high magnification image (b) corresponds to the FFT (c) . Scale bar corresponds to 50 nm.

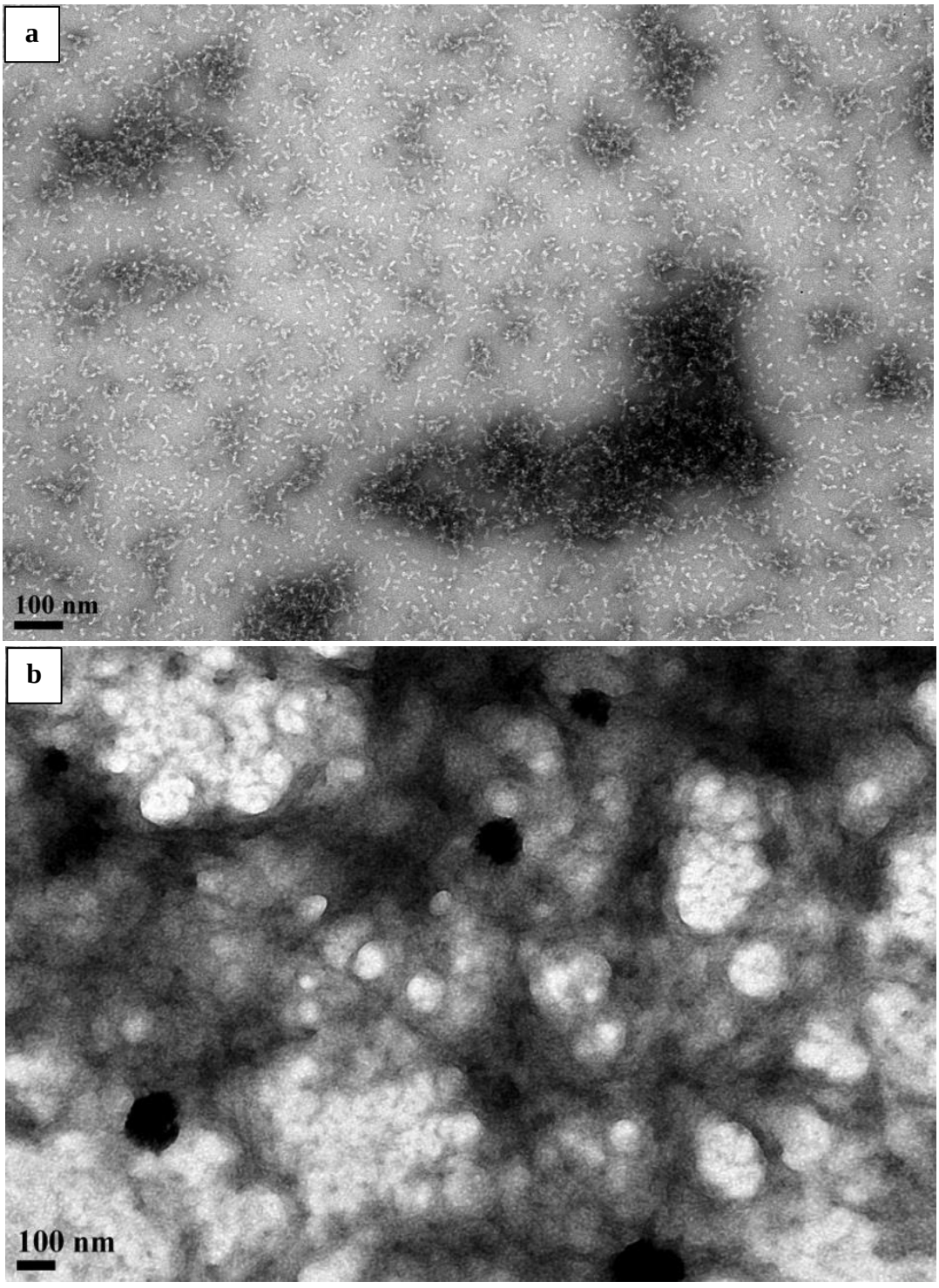

F**igure 8.** Representative images of precipitated protein and co-purified lipid. a) An example of precipitated mSPP at LPR = 0. b) An example of electron-dense membrane structures at LPR = 0 indicating co-purified endogenous lipid. Both scale bars correspond to 100 nm.

Table 2. Summary of conditions tested during 2D crystallization trials of mSPP. *Column 3 outlines the best set of conditions (buffer 1) identified for crystallizing 55-75% ASP cut mSPP. **Column 4 outlines the best set of conditions (buffer 2) identified for crystallizing non-ASP cut.

Parameters	**Range Tested**	***Buffer 1**	****Buffer 2**
pH	7.5	7.5	7.5
Protein Concentration (mg/ml)	0.1-1	1	1
ASP cut (%)	0-55%, 55-75%, 75-95%	55-75%	Non-ASP Cut
Lipid	DMPC (1 mg/ml and 10 mg/ml)	1 mg/ml	10 mg/ml
LPR (mol/mol)	0.25-120	10	40
Detergent	FC-12, Triton-X-100	FC12	FC12
Detergent Concentrations (%)	0.1-2.0	0.1	0.1
Temperature (ºC)	24, 28	24	24
Crystallization Technique	Dialysis tubing 14,000 MWCO	Dialysis tubing 14,000 MWCO	Dialysis tubing 14,000 MWCO
Buffer: HEPES (pH 7.5)	50 mM, 20 mM HEPES	50 mM HEPES	20 mM HEPES
NaCl (mM)	10-500	10	100
$MgCl_2$ (mM)	5	N/A	5
NaN_3 (mM)	5	N/A	5
Glycerol (%) (v/v)	20	20	20

CHAPTER 4

TWO-DIMENSIONAL CRYSTALLIZAITON OF SIGNAL PEPTIDE PEPTIDASE HOMOLOGUE FROM *Methanoculleus marisnigri* JR1 (MCMJRSPP)

4.1 Membrane morphologies and sizes of MCMJRSPP proteoliposomes and two-dimensional crystals

Batch 1 purified protein of MCMJRSPP reconstituted into exogenous lipid producing ideal membrane morphology over a range of LPRs (Table 3, D3-4). At LPRs ranging from 20 to 300, sheets, vesicles and tubular membranes were observed. Weak reflections were observed when membranes were assessed with an FFT to identify long-range order. Membrane sizes ranged from 100 nm to 10-15 μm in some instances (Figure 9a). At LPRs above 40, membrane morphology had a corrugated appearance potentially indicating ordered lipid crystallization (Figures 9b and c).

4.2 Two-dimensional crystallization of MCMJRSPP

Crystallization was detected after 9-12 days of dialysis at LPRs between 13 to 40. The dialysis timing was based on the CMC of n-Dodecyl-β-D-Maltopyranoside (DDM) (0.17mM) and 2D crystallization experiments described previously (19). Additionally, an extended dialysis time was used since the final concentration of DDM is unknown due to concentrating MCMJRSPP to the appropriate concentration with a 10 kDa MWCO amicon filter. The concentration of DDM prior to the final concentrating step is 0.05% (w/v).

Vesicles and sheets associated and unassociated with electron dense aggregates/membrane structures showed crystallinity (Figures 11, 12, 14, 16). LPRs above 20 showed a decrease in electron dense aggregates and crystallinity. For batches 4-6 and 8, crystallinity was detected within a narrow LPR range of 13 to 25.

4.3 Reproducibility of MCMJRSPP two-dimensional crystallization

Protein purification batches 4-6 and 8 reproducibly resulted in good membrane morphology that included sheets and vesicles (Table 3; Figures 11, 12, 14, 16). Amongst these four purifications in a narrow LPR range between 13 to 25, weak to strong reflections were observed (Figures 11, 12 and 14). In addition, high contrast crystalline patches were observed, starting with batch 4 (Table 4: D10-6). The high contrast crystalline patches were randomly dispersed in sheets and vesicles, ranging in size from 50 nm x 50 nm to 200 nm x 200 nm (Figures 11a-c). Images of negatively stained high contrast crystalline patches at high magnification showed strong first and second order reflections by FFT (Figures 11d and e). Batches 5, 6 and 8 also produced high contrast crystalline patches (Table 4: D13-6, D18-3, and D20-3). A summary of parameters tested is outlined in Table 4.

4.4 Two-dimensional crystallization buffer conditions

Buffers 2 and 3 were used to crystallize MCMJRSPP. Buffer 2 was tested for dialysis experiments 1-8 and 10-15. Batch 1 under buffer 2 conditions produced membranes. However, batches 2 and 3 did not reproduce these results. New lipid preparations were compared and ruled out as possible sources for the discrepancies observed. Buffer 3, replacing 20 mM HEPES [pH 7.5] in buffer 2 with 20 mM MES [pH 6.0], was utilized to

determine if batches 2 and 3 would crystallize under slightly different buffer conditions. Batch 2 under buffer 3 conditions (Table 3, D9-2) produced good membrane morphology and strong reflections (Figures 10a and b). However, under the same conditions batch 3 (Table 3, D9-6) did not yield the same results. Following these results, it was determined that a buffer exchange, following the purification before the gel filtration step differed. This difference was corrected in subsequent purifications. It was determined that buffer 3 produced comparable or better membrane morphologies and high contrast crystalline patches compared to buffer 2.

4.5 Projection maps of MCMJRSPP.

Electron micrographs of negatively stained high contrast crystalline patches from dialysis conditions D10-6 and D18-3 were processed with 2dx (47) to produce projection maps. Images 17b and d were processed and produced the projection structures and maps seen in Figures 17a, c, d, and f. The unit cell dimensions are a = 178 Å, b = 160 Å, γ = 92 Å and a = 175 Å, b = 167 Å γ = 92 Å (Table 5), respectively. Both projection maps have p1 symmetry and are limited to 16 Å resolution due to the stain.

The monomer dimensions for D10-6 are approximately 80 Å by 75 Å.The measurements for D18-3 are approximately 70 Å by 70 Å. These dimensions are based on preliminary projection maps. Three strong densities appear to represent monomers. In both projection maps, low-contrast, elongated densities protrude from each monomer.

4.6 Discussion

The LPR was pivotal to obtaining 2D crystals of MCMJRSPP. Broad ranges of membrane morphologies and sizes were observed at LPRs between 1 to 300 during MCMJRSPP crystallization trials (Table 3 and 4). The best results with batch 1 were obtained at LPR = 40. From these initial crystallization trial results, it was determined

that crystallinity increased as the LPR decreased. Additional batches (4-6 and 8) showed reproducibility at LPR = 40 and lower LPRs between 13 to 25. The narrow range of LPRs between 13 to 25 produced high contrast crystalline patches indicating MCMJRSPP crystallizes in an LPR-dependent manner. LPR-dependency has been observed previously with membrane proteins (48).

Two buffers were tested during the crystallization of MCMJRSPP. Buffer 2 was formulated based on previous 2D crystallization with 20% glycerol (49, 50, 51), along with previous dialysis trials using mSPP (HEPES, NaCl, and pH), and buffer components (MES and NaN_3) (52).

Buffer 2 worked well with batch 1 but not with purified protein from batches 2 and 3. Dialysis was repeated again for these two batches to rule out human and lipid preparation error. In addition, the protein purification protocol was reviewed to identify any discrepancies between purification batches 1, 2 and 3. While other possibilities for error were being ruled out, the buffer components were changed slightly, MES was substituted for HEPES and the pH was changed from 7.5 to 6.0 to create buffer 3 (52). Batches 2 and 3 were dialyzed against buffer 3 conditions and it was found that batch 2 showed decent membrane morphology (less than 1 μm to several microns in size) with weak to good reflections while batch 3 did not. Following success with buffer 3, both buffers were tested until it was determined that buffer 3 gave better results in terms of membrane morphology and crystallinity (Table 3: D14-5 and D14-6). Dialysis 14-5 under buffer 2 conditions at LPR = 20 produced vesicles and sheets less than 50 nm to 1 μm in size and did not contain high contrast crystalline patches. In contrast dialysis 14-6 under buffer 3

conditions and at the same LPR produced vesicles and sheets that measured less than 50 nm to 1-2μm and contained high contrast crystalline patches.

Membrane morphology for MCMJRSPP crystallization trials varied greatly with high LPRs (above 40) producing vesicle, sheet and tubular morphologies that were less than a 50 nm to 10-15 μm in length. However, as the LPR decreased, smaller membrane morphologies were observed, less than 50 nm up to 1-2 μm. With the decrease in LPR, two types of crystalline regions were observed within membrane sheets and vesicles. Visible high contrast crystalline patches were observed in 10 to 20% of vesicles and sheets at a nominal magnification of 40,000 to 60,000x. The other type of crystallinity was only evident when membranes were scanned with an FFT in Digital Micrograph.

It is unclear how the high contrast crystalline patches are forming within vesicles and sheets. The patches do not appear to be a moiré due to two lattices based on observations of the FFTs. The membranes do not appear to be stacked and there is an absence of multiple edges to indicate that such an event is occurring.

The best crystals were observed when there was a presence of aggregate. The aggregate would have vesicles attached around the perimeter of its electron dense structure (Figure 16a). Within these vesicles and sheets, attached to or scattered around the aggregate, high contrast crystalline patches were observed that showed first and second order reflections (Figure 14).

During the crystallization trials two aspects of the purification process impacted the dialysis results. The first was noted during the purification of batches 2 and 3 of

MCMJRSPP. Batch one was eluted from a Ni-NTA column and a buffer exchange was completed before gel filtration. However, for batches 2 and 3, a buffer exchange was not completed which impacted the reproducibility. The absence of the buffer exchange may have negatively impacted the pH or dialysis buffer components.

The other aspect that impacted crystallization conditions appears to have been the use of a new batch of n-dodecyl-β-D-maltopyranoside (DDM) detergent. Batch 7 purification was completed with a new batch of DDM. Dialysis of batch 7 resulted in aggregate and no vesicles. These results were similar to LPRs lower than 13 tested with previous batches where the grid squares contain mostly aggregate and no vesicles.

For batches tested prior to batch 7, as the LPR is increased over 13, more vesicles appeared associated and unassociated with the electron dense aggregate. Eventually, as the LPR surpasses 20, vesicles were present on the grid with very little aggregate. Upon testing of high LPRs (20, 25 and 30) for batch 7, it was theorized the optimal LPR for batch 7 was slightly increased due to a new batch of DDM. The new DDM most likely succeeded in removing more bacterial lipid during purification than the previous batch.

MCMJRSPP was dialyzed for 9 to 12 days to completely removed DDM by dialysis. The reason for the long dialysis is due to the low critical micelle concentration of DDM. Other researchers using DDM to solubilize membrane proteins have found DDM removal takes 12-13 days using dialysis blocks and exchanging dialysis buffer daily (53). The daily buffer exchanges were necessary due to the small amount of buffer that can be contained within the dialysis block. In the case of MCMJRSPP, dialysis blocks were not used. A volume of 300 ml was used in all dialysis trials.

If detergent is not adequately removed during dialysis, the detergent will degrade membranes and crystals over time. An excess of detergent can easily be tested by aliquoting 2 µl of dialysate onto a grid and observing how the drop spreads over the grid.

Protein purifications of MCMJRSPP contained co-purified lipid (Table 4, far right column). The presence of co-purified lipid did not seem to have a substantial effect on the LPR. All other batches tested at LPR = 0 showed membrane structures. Based on the reproducibility between batches, 4-6 and 8, the amount of endogenous lipid appears to be similar between batches and did not have a significant influence on the outcome of crystallization trials investigated thus far, as the optimal LPR to produce both membranes and crystals is a narrow range between 13-25.

It is unclear whether or not the amount of lipid had a significant impact on the spacing of the protein in the projection maps. More images will be processed at different LPRs to determine whether this variable contributes to an increased packing density of MCMJRSPP.

Table 3. 2D crystallization parameters for different purification batches of MCMJRSPP. *Batches 2 and 3 (B2 and B3) were purified differently compared to the other batches (see discussion). **Batch 7 (B7) was solubilized and purified using a new bottle of DDM (see discussion).

*Dialysis	Protein Purif. Batch	LPR (mol/ mol)	Buffer Cond.	Dialysis Time (days)	Results	LPR = 0 Results
D3-4	B1	40	Buffer 2	10	Vesicles, less than 50 nm to microns. Lipid crystals. Weak reflections. Figure 9	Precipitated protein/ No aggregate. Bacteria present
D9-2	B2*	40	Buffer 3	10	Vesicles and sheets, less than 50 nm to microns. Weak reflections. Figure 10	Co-purified lipid/No precipitated protein
D9-6	B3*	40	Buffer 3	10	No membranes. Figure 10	Co-purified lipid/No precipitated protein
D10-6	B4	20	Buffer 2	10	Vesicles, less than 50 nm to microns. High contrast crystalline patches randomly dispersed in vesicles. Strong reflections. Figure 11	Co-purified lipid/No precipitated protein
D12-6	B4	15	Buffer 3	12	Vesicles and sheets, less than 50 nm to 2 μm. High contrast crystalline patches. Strong reflections. Vesicles associated and unassociated with e-dense aggregates. Figure 12	Co-purified lipid/No precipitated protein
D13-7	B5	15	Buffer 3	11	Vesicles, less than 50 nm to microns. High contrast crystalline patches. Strong reflections. Vesicles associated and unassociated with electron dense aggregates. No Figures	Co-purified lipid/No precipitated protein
D14-5	B6	20	Buffer 2	12	Vesicles less than 50 nm to 1 μm. No high contrast crystalline patches observed. Weak reflections. Vesicles unassociated and associated with electron dense aggregate. Figure 13	N/A
D14-6	B6	20	Buffer 3	12	Vesicles, less than 50 nm to 1-2μm. High contrast crystalline patches. Strong reflections. Vesicles associated and unassociated with minimal electron dense aggregates. Figure 13	N/A
D18-3	B6	18	Buffer 3	12	Vesicles and sheets, less 50 nm to 1-2 μm. High contrast crystalline patches. Strong reflections. Vesicles associated and unassociated with electron dense aggregates. Figure 14	N/A
D17	B7**	20	Buffer 3	12	Electron dense aggregate. Figure 15	Co-purified lipid/No precipitated protein
D19	B7**	35	Buffer 3	12	Electron dense aggregate with minimal membrane vesicles, less than 500 nm. Figure 15	Co-purified lipid/No precipitated protein
D20-3	B8	20	Buffer 3	12	Vesicles, less than 500 nm. High contrast crystalline patches. Strong reflections. Vesicles associated and unassociated with electron dense aggregates. Figure 16	Co-purified lipid/No precipitated protein

Table 4. Summary of conditions tested during 2D crystallization trials of MCMJRSPP. *Column 3 outlines the best combination of conditions (buffer 3) identified for crystallizing MCMJRSPP.

Parameters	Range Tested	Buffer 3*
pH	7.5 and 6.0	6.0
Protein Concentration (mg/ml)	0.5 mg/ml	0.5 mg/ml
Protein Purification Batches	1-8	6
Lipid (10 mg/ml) in 3.5% Na-DOC	DMPC	DMPC
LPR (mol/mol)	1 - 300	13-25
Detergent	DDM	DDM
Temperatures (ºC)	24ºC	24ºC
Dialysis Time (days)	9-12	9-12
Crystallization Technique	Dialysis tubing 14,000 MWCO	Dialysis tubing 14,000 MWCO
Buffer 2 HEPES (pH 7.5) and Buffer 3 MES (6.0)	20 mM HEPES, 20 mM MES	20 mM MES
NaCl (mM)	100	100
$MgCl_2$ (mM)	5	5
Glycerol (%) (v/v)	20	20
NaN_3 (mM)	5	5

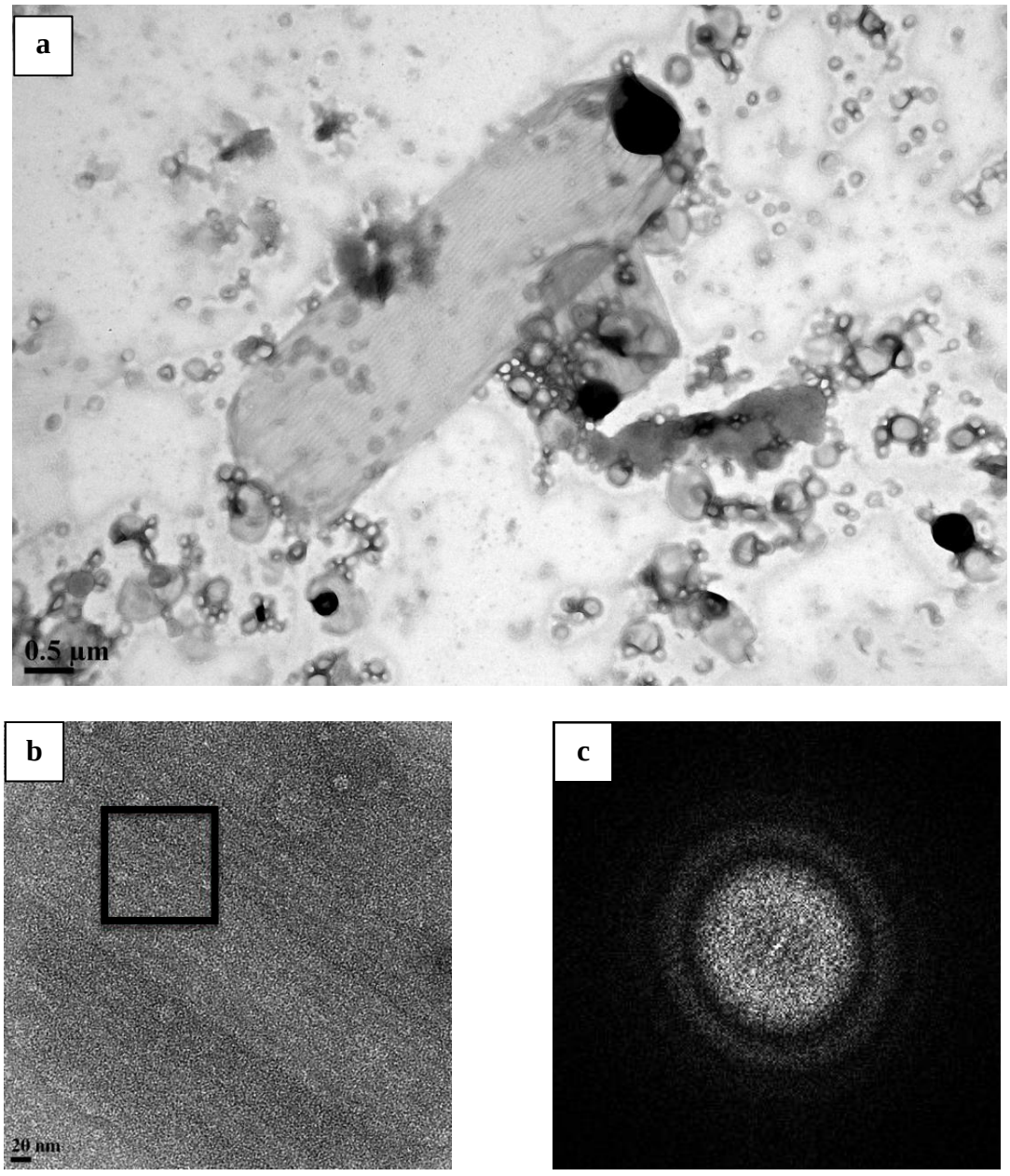

Figure 9. 2D crystallization trial of MCMJRSPP dialysis 3-4. a) Representative overview image of batch 1 reconstituted at LPR = 40 under buffer 2 conditions. Vesicles and tubular morphologies ranged in size up to from less than 1 µm to many microns in length. Scale bar corresponds to 0.5 µm. b and c) High magnification of vesicle showing a corrugated pattern with FFT. The boxed area in the high magnification image (b) corresponds to the FFT (c). Scale bar corresponds to 20 nm.

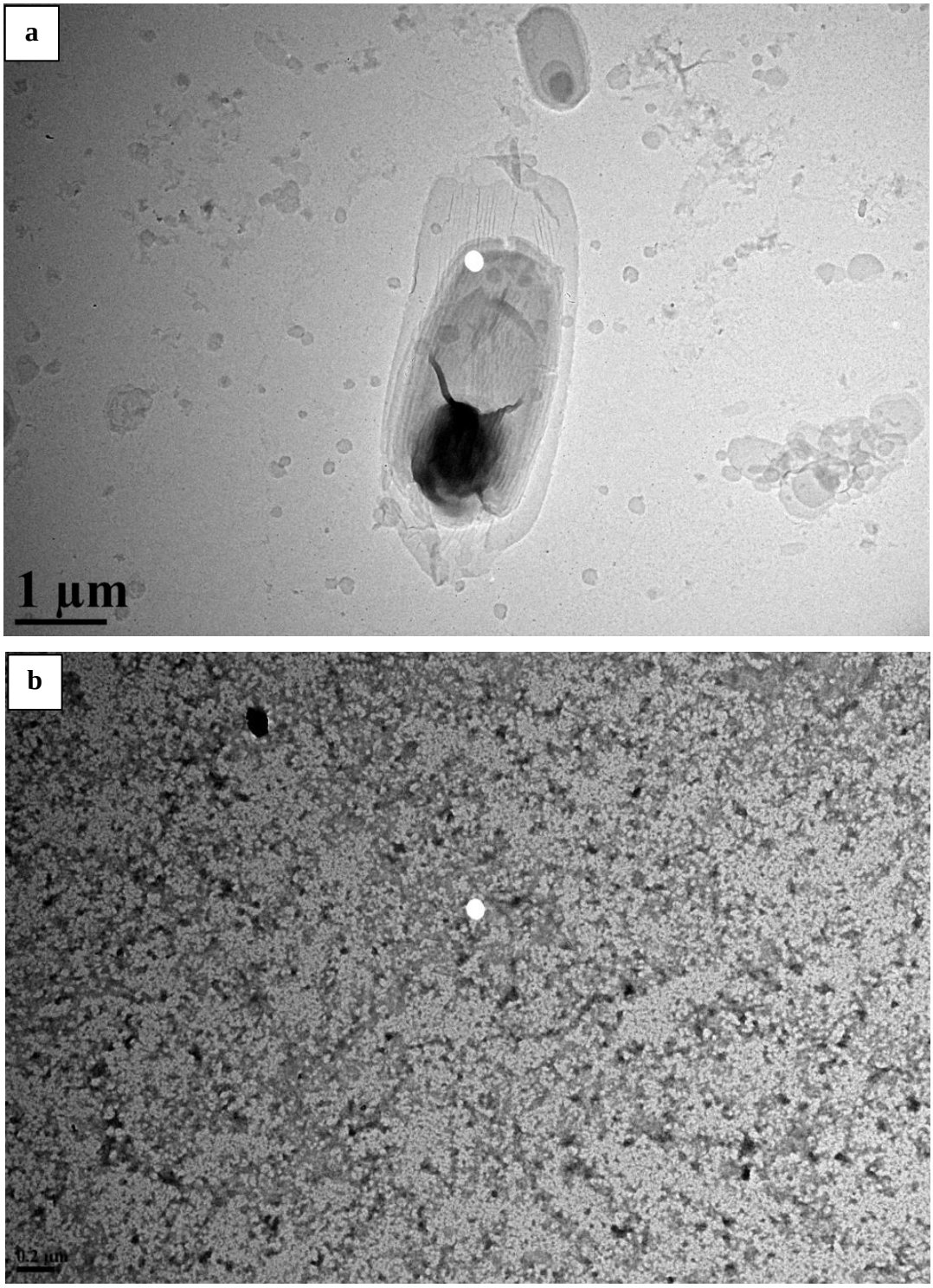

Figure 10. 2D crystallization trial of MCMJR SPP dialysis batch 2 compared to batch 3 under the same conditions at LPR = 40 using buffer 3. a) Representative image of batch 2. Scattered vesicles and sheets ranging in size. Scale bar corresponds to 1 µm. b) No vesicles or sheets were observed in Batch 3 under the same conditions. Scale bar corresponds to 0.2 µm.

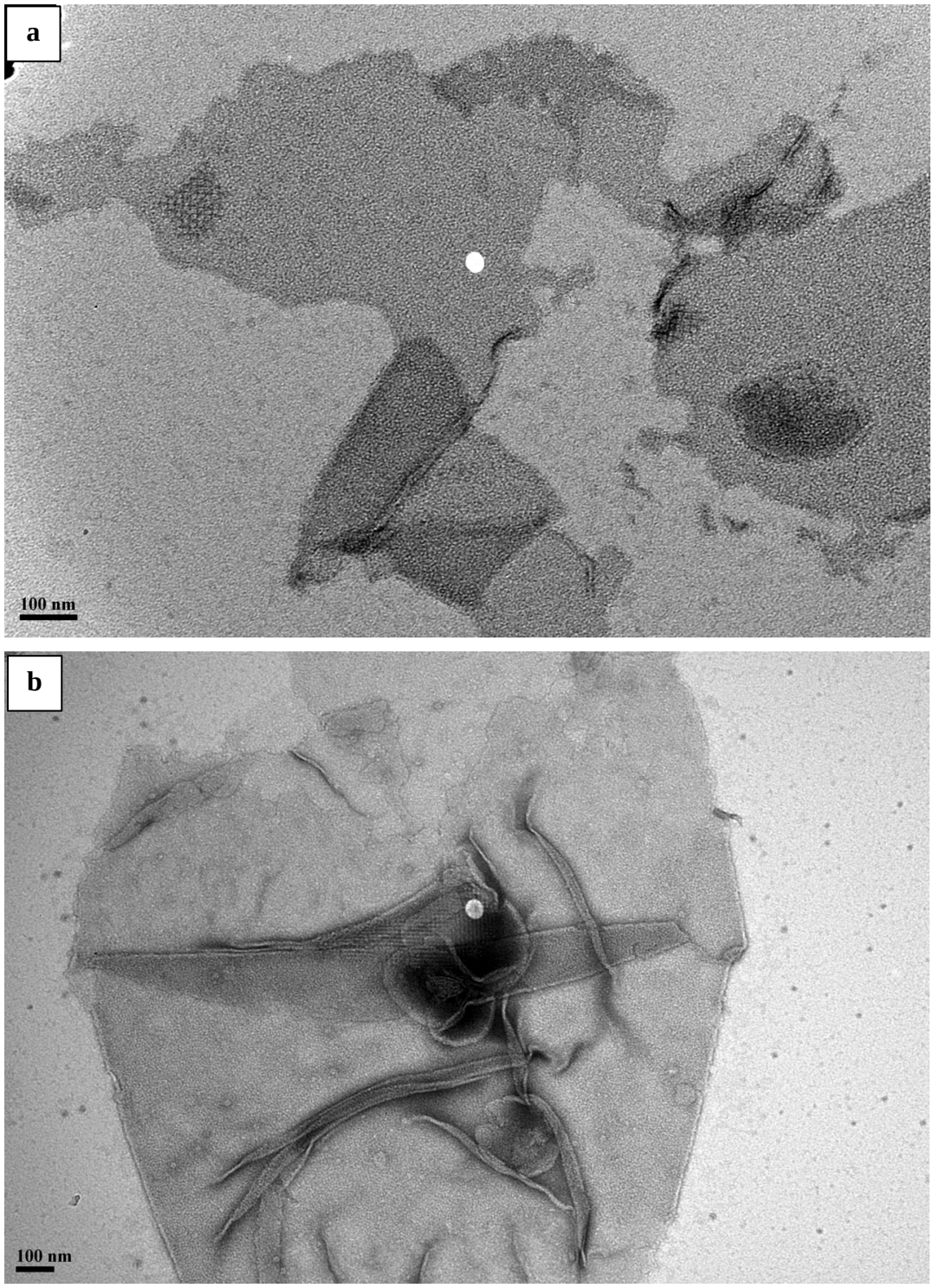

Figure 11. 2D crystallization trials of MCMJR SPP dialysis 10-6. a-c) Overview images of batch 4 at LPR = 20 under buffer 2 conditions. Sheets and vesicles are seen with high contrast crystalline patches present. Scale bars correspond to 100 nm (a, b) and 0.5 μm (c). d) High magnification image of area circled in overview (c). Scale bar corresponds to 20 nm. e) FFT showing strong first and second order reflections (e). The boxed area in the high magnification image (d) corresponds to the FFT (e).

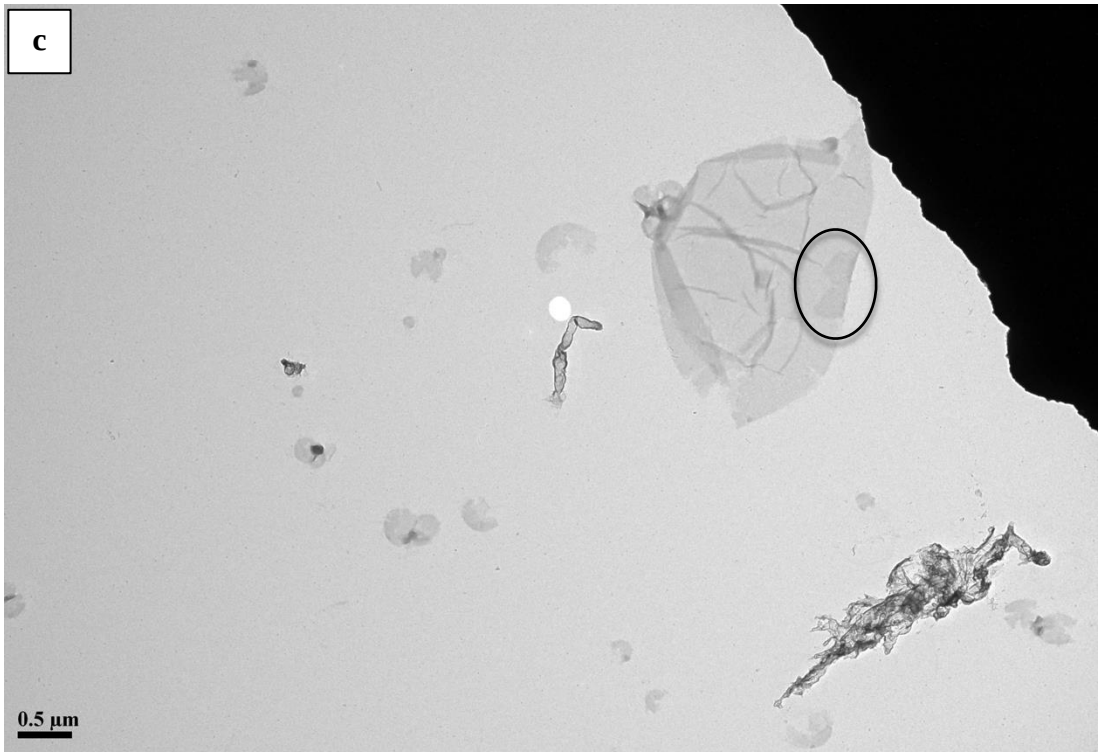

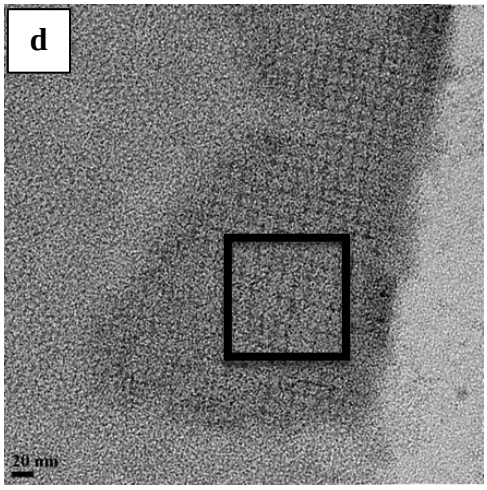

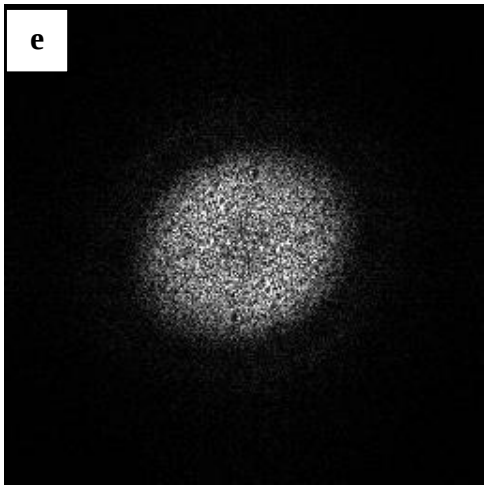

Figure 11 continued

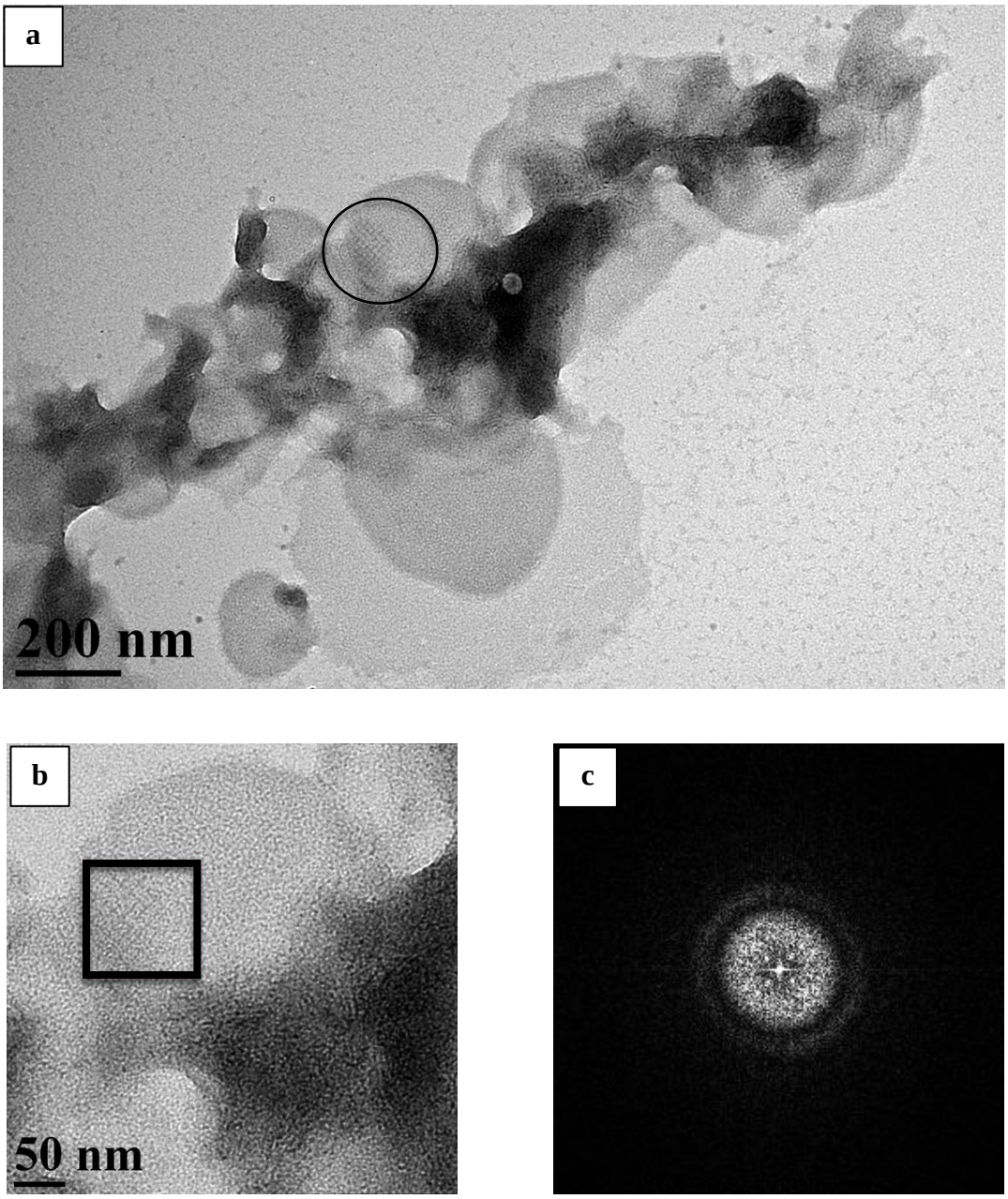

Figure 12. 2D crystallization trials of MCMJRSPP dialysis 12-6. a) Overview image of batch 4 crystallized at LPR = 15 under buffer 2 conditions. Vesicles and sheets are seen attached to electron dense aggregate. Circled area shows high contrast crystalline patch. Scale bar correspond to 200 nm. b) High magnification image of circled area. c) FFT showing strong reflections of high contrast crystalline patch. The boxed area in the high magnification image (b) corresponds to the FFT (c). Scale bar corresponds to 50 nm.

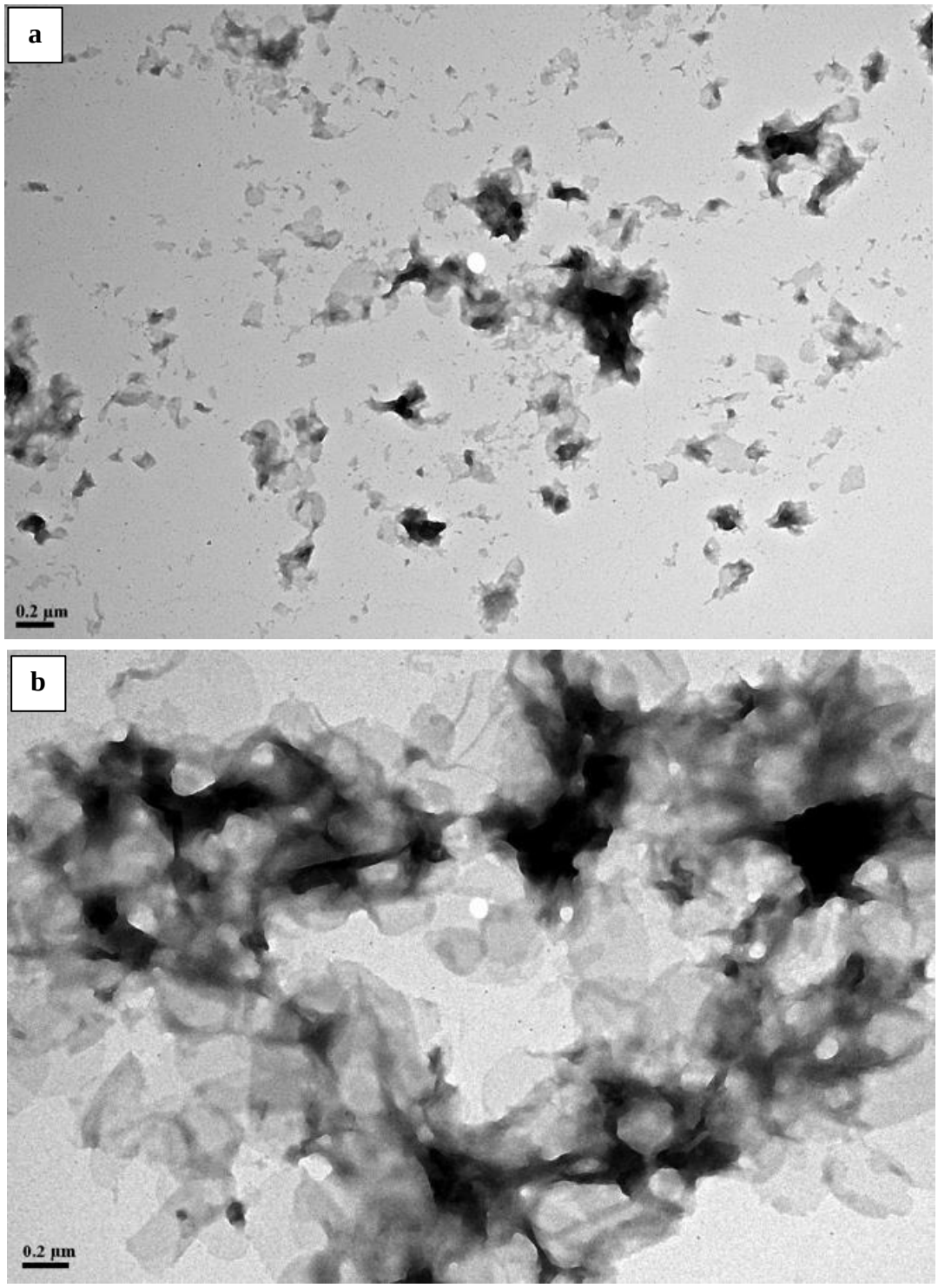

Figure 13. 2D crystallization trials of MCMJRSPP dialysis 14-5 and 14-6. a) Representative overview image of batch 6 at LPR = 20 under buffer 2 conditions compared to overview image of batch 6 at LPR = 20 under buffer 3 conditions (b). Buffer 3 shows an increase in membrane morphologies compared to results from buffer 2. Scale bars correspond to 0.2 µm.

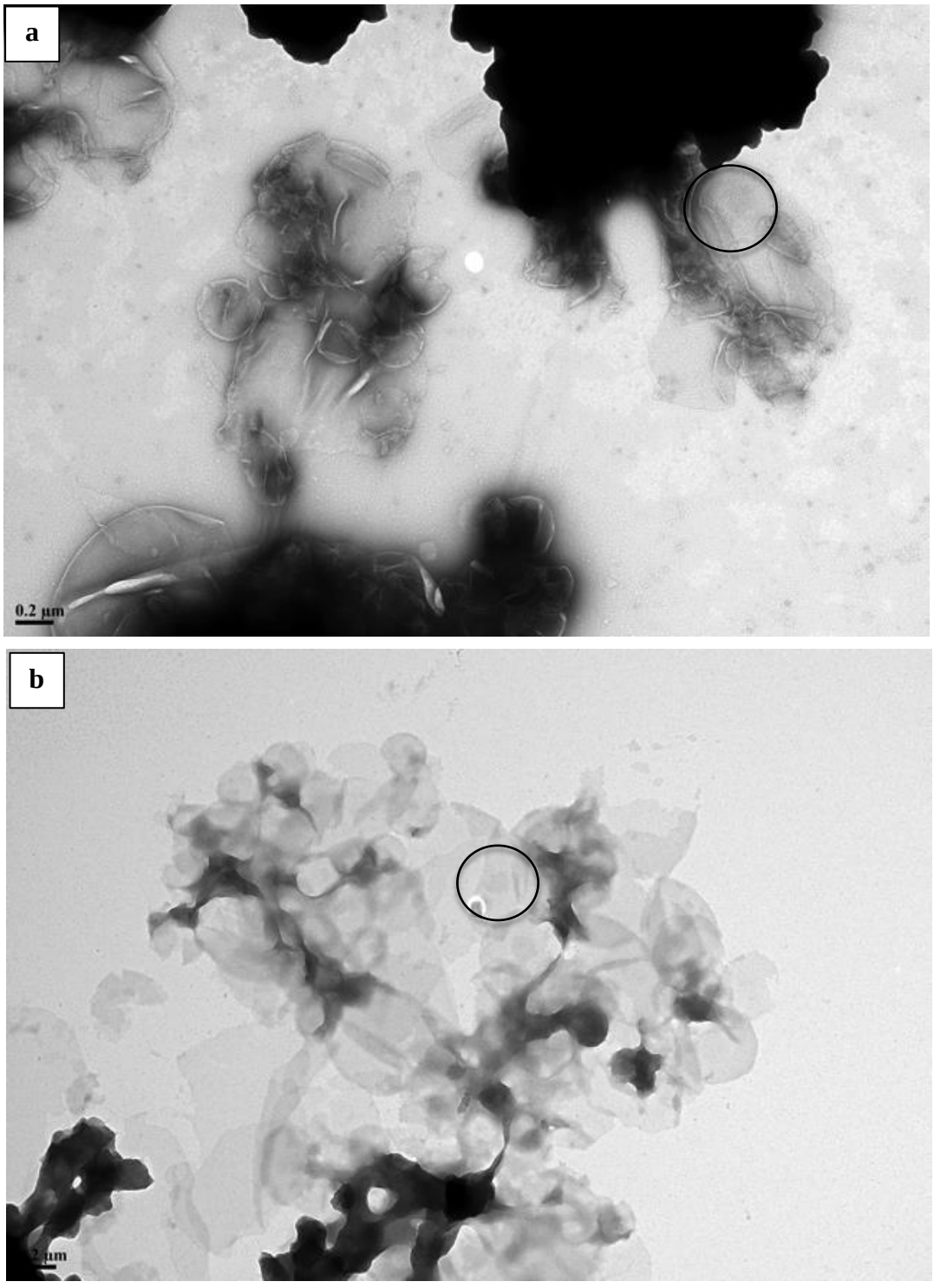

Figure 14. 2D crystallization trials of MCMJRSPP dialysis 18-3. a and b) Representative overviews of batch 6 at LPR = 18 under buffer 3 conditions. Scale bar corresponds to 0.2 µm. c-f) High magnification images with high contrast crystalline patches. The boxed areas in the high magnification images (c and e) correspond to the FFTs (d and f). Scale bar corresponds to 20 nm. FFTs show strong first and second order reflections.

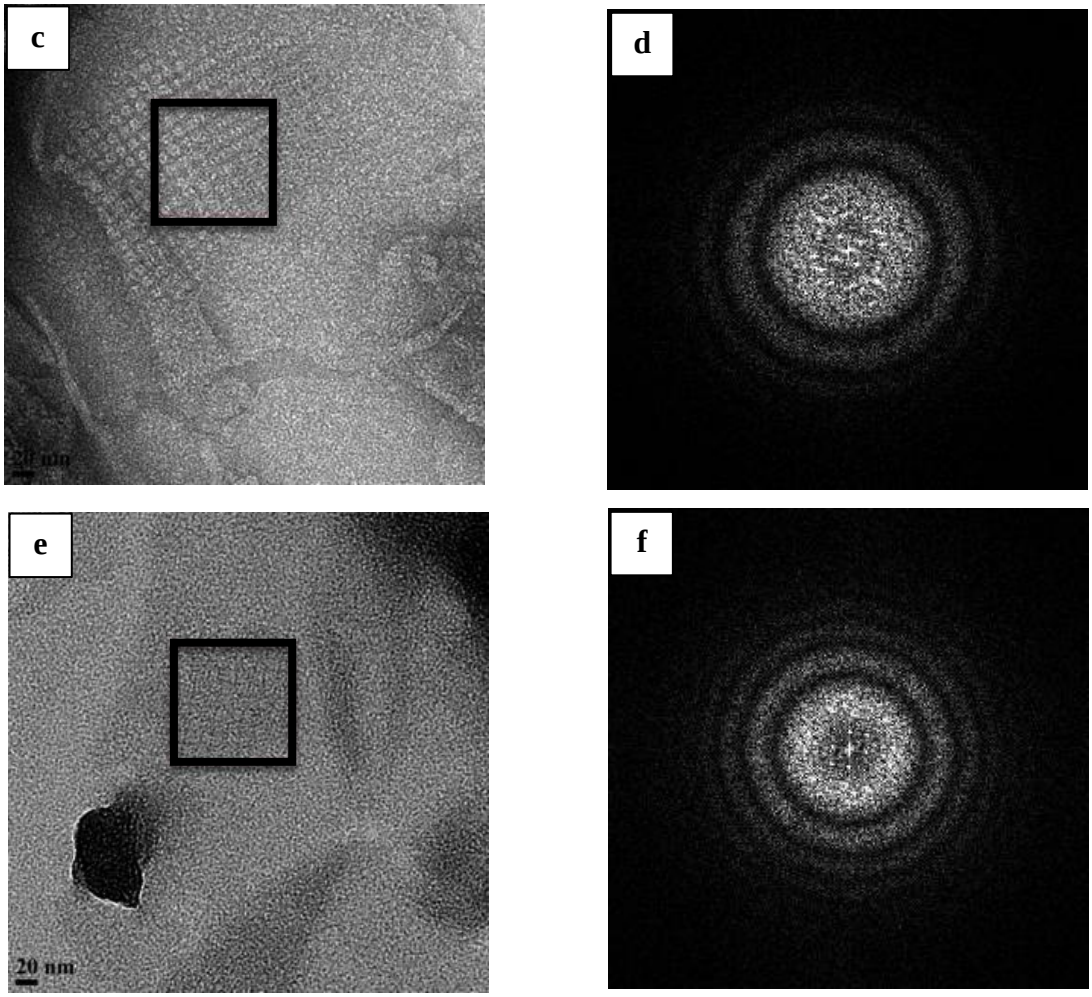

Figure 14 continued.

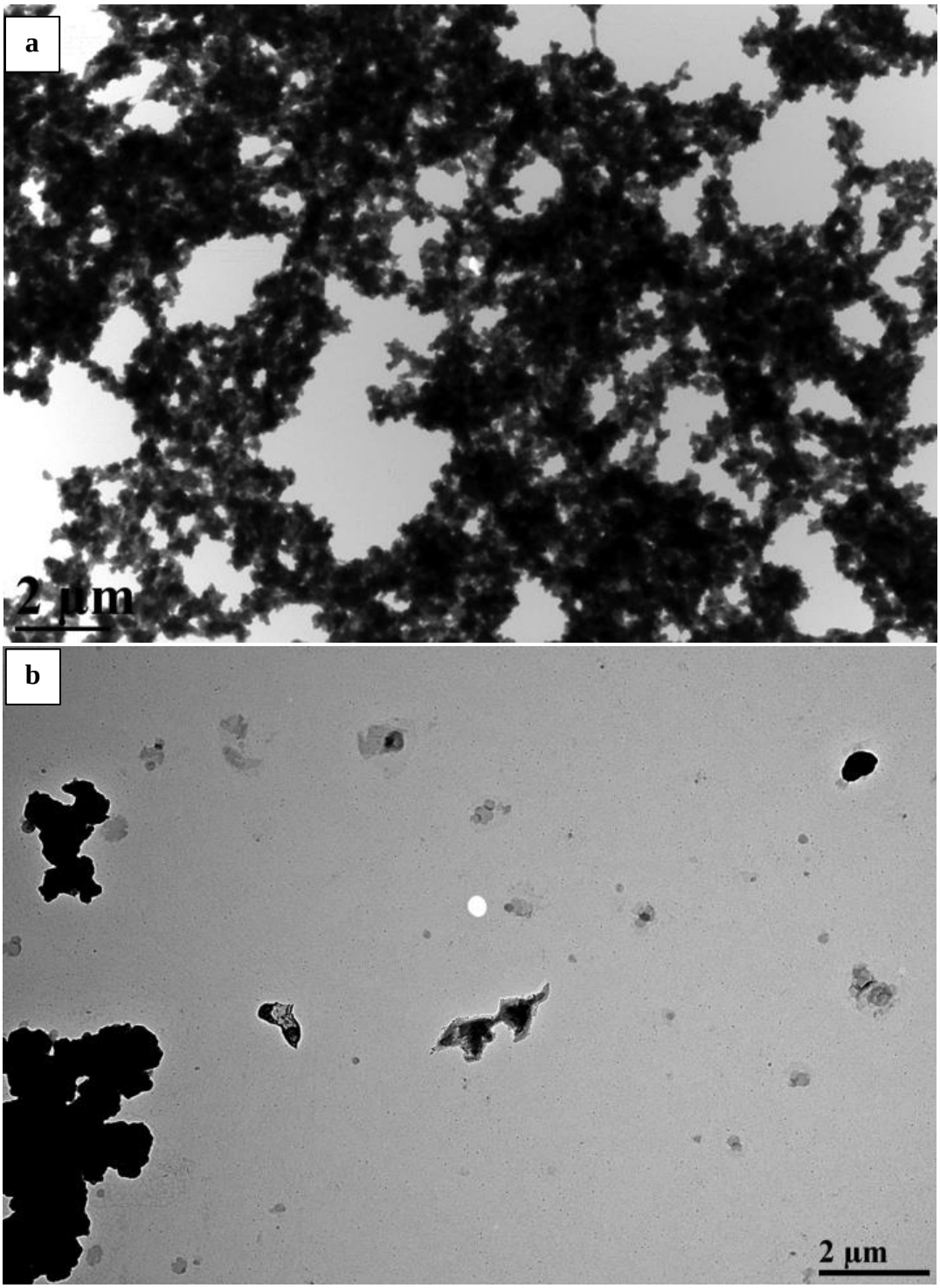

Figure 15. 2D crystallization trials of MCMJRSPP dialysis 17-1 and 19-3. a) Representative overview image of 17-1 at LPR = 20 under buffer 3 conditions. Increase in membrane structures compared to previous batches dialyzed at LPR = 20. b) Dialysis 19-3 shows an increase in vesicles compared to 17-1. The LPR was increased from 20 to 35. The skewed LPR resulted from additional endogenous co-purified lipid being removed due to a new bottle of DDM. Scale bars correspond to 2 µm.

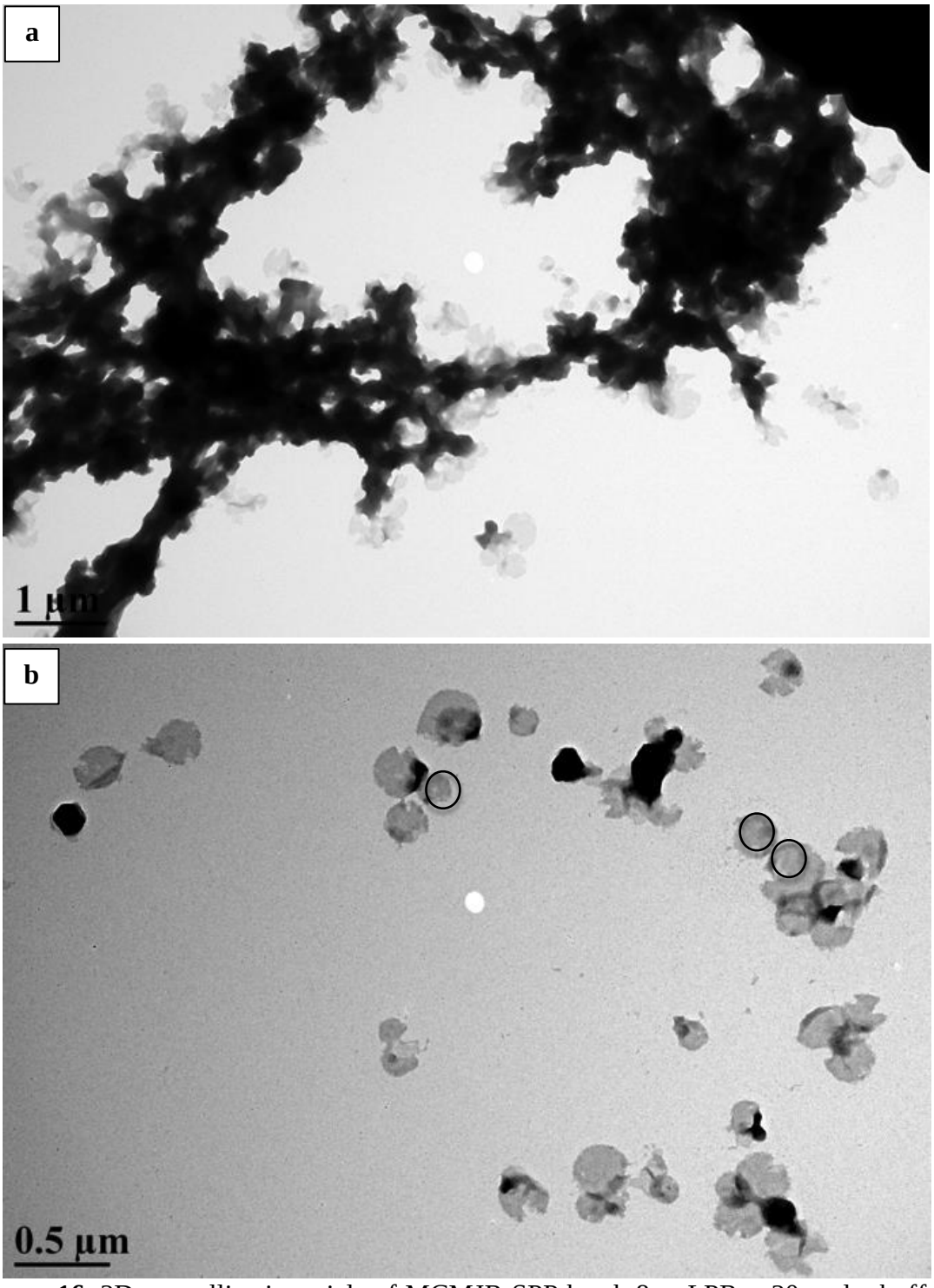

Figure 16. 2D crystallization trials of MCMJR SPP batch 8 at LPR = 20 under buffer 3 conditions. a) Vesicles associated and unassociated with electron dense aggregate. Scale bar corresponds to 1 µm. b) Vesicles with high contrast crystalline patches (circles). Scale bar corresponds to 0.5 µm.

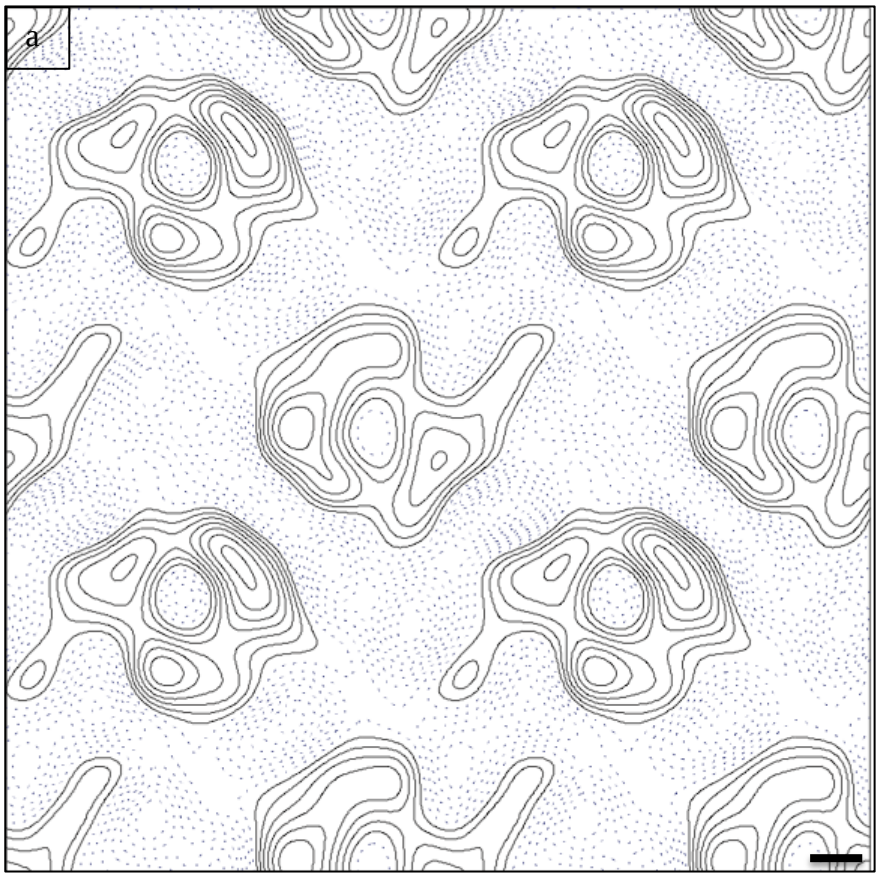

Figure 17. Projection map of MCMJRSPP dialysis 10-6 and 18-3 a) Shows the projection map to 16Å. The unit cell dimensions are *a* = 178 Å, *b* = 160 Å, ɣ = 92 Å. Three strong densities can be seen in the projection map around the pore. Scale bar corresponds to 20 Å. b) Negatively stained crystalline MCMJRSPP vesicle. High contrast crystalline lattice is visible within in the membrane of the vesicle. Scale bar corresponds to 20 nm. c) Shows the resulting projection structure. d) Shows the projection map to 16 Å resolution. The unit cell dimensions are *a* = 175 Å, *b* = 167 Å, ɣ = 92 Å. Three strong densities can be seen in the projection map with a minute pore. Scale bar corresponds to 20 Å. e) A negatively stained crystalline MCMJRSPP vesicle. Scale bar corresponds to 20 nm. f) Shows the resulting projection structure.

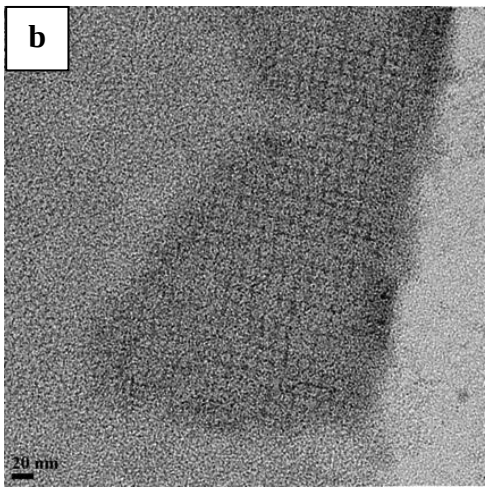

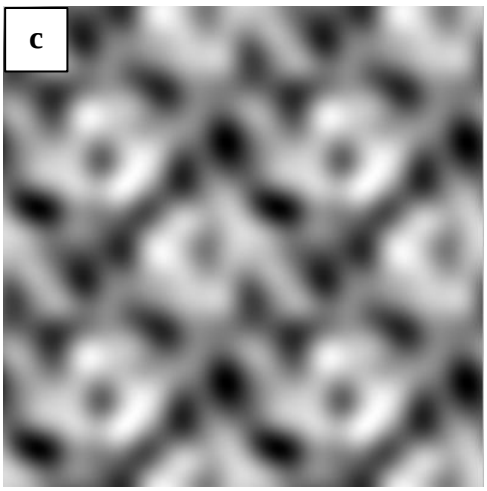

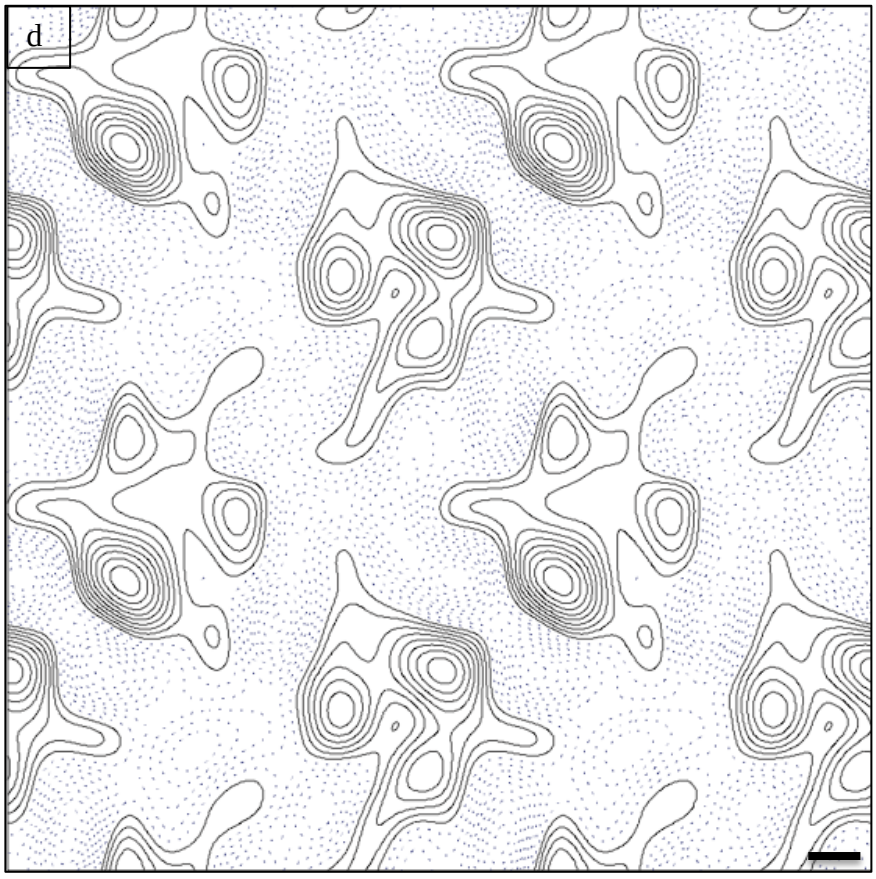

Figure 17 continued.

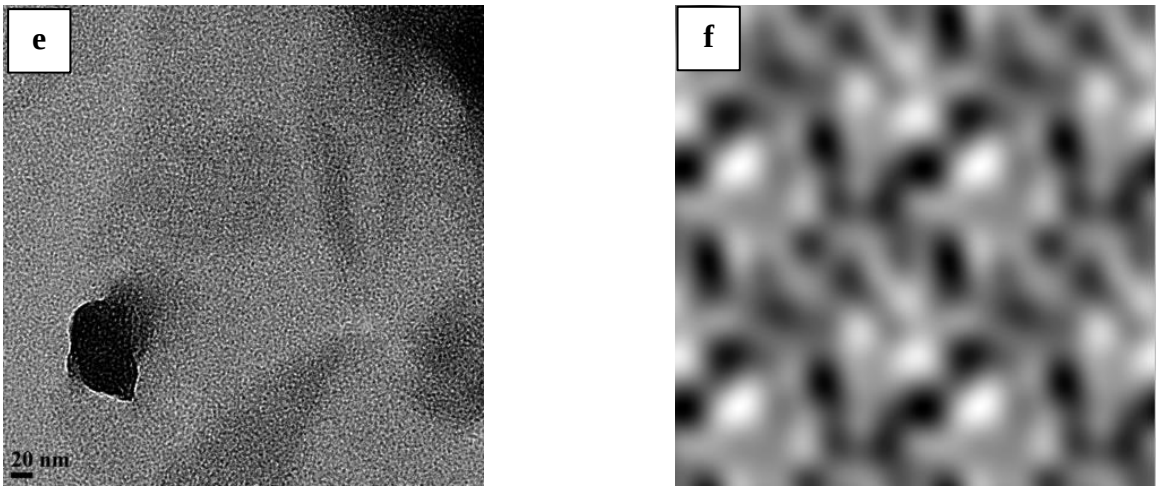

Figure 17 continued.

Table 5. Electron crystallographic data for MCMJRSPP D10-6 and D18-3.

Electron Crystallographic Data for D10-6 and D18-3	
Imaging Conditions	
Nominal magnification / camera length (cm)	65431.4 / 100
High Tension (kV)	120
Electron Source	Tungsten
Defocus (Å) D10-6 Defocus (Å) D18-3	x = 22293.3, y = 20983.9 x = 10524.6, y = 13925.3
Astigmatic (deg.) D10-6 Astigmatic (deg.) D18-3	57.04 23.92
Image Processing	
Scan Area (pixels)	2048 x 2048
Pixel Size (μm)	14
Program System	2dx
Crystal Parameters	
Unit cell (Å; deg.) D10-6 Unit cell (Å; deg.) D18-3	a = 178, b = 160, γ= 92 a = 175, b = 167, γ= 92
Projection Symmetry	p1

CHAPTER 5

DISCUSSION

Electron crystallography was used to investigate achaea aspartyl protease SPPs from *Haloarcula morismortui* and *Methanoculleus marisnigri* JR1. This is the first time an SPP homologue has been crystallized in 2D. It was shown that MCMJRSPP reproducibly crystallized within a narrow LPR range of 13 to 25 under specific buffer conditions (Table 4). Within this narrow LPR range, high contrast crystalline patches were observed and processed using 2dx (47). In contrast to MCMJRSPP, high contrast crystalline patches were not observed in any of the conditions tested for mSPP. Overall, mSPP showed limited success during 2D crystallization trials. Optimizing dialysis conditions using MCMJRSPP may potentially provide insight and facilitate reproducible and improved crystallization of mSPP.

DMPC was utilized for both mSPP and MCMJRSPP. The lipid, solubilized in detergent, is added based on the LPR calculations (see methods) to the detergent-solubilized protein. As the detergent is removed during dialysis, the membrane proteins will reconstitute into a lipid bilayer. When no lipid is added, the membrane proteins will either precipitate as the detergent is dialyzed, or it will form aggregates, membrane structures, and/or electron dense amorphous structures indicating co-purified lipid. The presence of aggregates and membrane structures indicate that not all of the endogenous lipid was removed during the purification process. Ideally, as much endogenous lipid as possible should be removed prior to starting crystallization trials. In both crystallization trials, co-purified lipid was present. Only in the case of MCMJRSPP, did the presence of

endogenous lipid not appear to have a substantial effect on reproducibility. In attempts to reproduce membrane morphology and crystallinity observed with dialysis 14-3 for mSPP, multiple batches of 55-75% ASP cut mSPP produced different results within a narrow LPR range and at the same LPR.

The protein concentration was kept constant at 0.5 mg/ml for all crystallization conditions involving MCMJRSPP. Future tests will involve varying the protein concentration. Unlike MCMJRSPP, wide ranges of protein concentrations were tested for mSPP from 0.1-1 mg/ml. None of these variations contributed to remarkable changes. Other groups have found that testing a range of protein concentrations is critical; such was the case with secondary citrate/sodium symporter CitS (54, 55).

Images of negatively stained crystals for MCMJRSPP were processed using 2dx (47). The following unit cell dimensions were calculated; a = 178 Å, b = 160 Å, ɣ = 92 Å and a = 175 Å, b = 167 Å ɣ = 92 Å (Table 5). Both projection maps have p1 symmetry (no symmetry imposed) and are limited to 16 Å resolution because they are negatively stained. Negative stain imposes a limit on the resolution by surrounding and coating the protein crystal. Electron cryo-microscopy is used to collect higher frequency data because the sample is in frozen hydrated buffer and data is collected under low does conditions. The monomer dimensions for Figures 17 a and d were 80 Å by 75 Å and 70 Å by 70 Å.

There are currently two 3D structures of aspartyl proteases related to mSPP and MCMJRSPP. The presenilin homolog (PSH) variant determined by X-ray crystallography to 3.3 Å resolution (32) and human SPP determined by signal particle analysis (31).

PSH was purified from *Methanoculleus marisnigri* JR1 and was engineered to contain mutations and loop deletions to improve stability in solution and crystallization; this however did not affect protease activity. The total molecular weight of PSH was approximately 158 kDa, indicating oligomerization. Li and colleagues calculated the following dimensions for one molecule of PSH; 50 Å in length, 40 Å in width and height (32). In comparison, a monomer of MCMJRSPP had slightly larger dimensions (70 Å by 80 Å) compared to a monomer of PSH (50 Å x 40 Å). Both MCMJRSPP and PSH are from the same archaeon bacterium, *Methanoculleus marisnigri* JR1. The difference in size could be related to the sequence engineering that was necessary to crystallize PSH. Five missense mutations were introduced mostly in the surface loops; these loops were also subjected to proteolysis by V8 protease. These mutations and loop deletions did not affect PSH protease activity.

Single particle analysis showed a homotetramer, which is active *in vitro* (31). Given the absence of a lipid bilayer and potentially due to signal particle analysis used, the homotetramer may not be the active structure *in vivo*. Previous work has shown that endogenous human SPP functions as an active dimer *in vivo* (30). Miyashita and colleagues showed DDM-solubilized SPP produces a single band at 200 kDa in a Blue-Native PAGE, indicating a multimeric complex like PSH. Additional Blue-Native PAGE data of DDM-solubilized *Drosophila* SPP showed a band at 180 kDa, indicating that *Drosophila* SPP forms a multimeric complex similar to human SPP (31).

The bullet shaped homotetramer of human SPP measures 85 Å in length and width and 130 Å in height. In comparison, MCMJRSPP has slightly shorter dimensions than human

SPP. MCMJRSPP is an archaeal SPP and may be structurally different compared to the human SPP described by Miyashita and colleagues.

CHAPTER 6

CONCLUSION/FUTURE DIRECTIONS

Archaeal homologues of SPP, MCMJRSPP and mSPP were crystallized in 2D. MCMJRSPP crystallized in an LPR-dependent manner, forming high contrast crystalline patches. These crystalline patches measured up to 200 nm x 200 nm and showed unit cell measurements of a = 178 Å, b = 160 Å, ɣ = 92 Å and a = 175 Å, b = 167 Å ɣ = 92 Å. Projection maps at 16 Å resolution showed three electron densities per monomer. Based on the preliminary projection maps, MCMJRSPP may be a dimer. Further optimization is planned to obtain larger lattices for processing and for collecting cryo-EM data to determine the structure at higher resolution and in 3D.

Additional crystallization trials are necessary to determine whether the crystallization conditions for MCMJRSPP are applicable to mSPP crystallization. Preliminary data appears to indicate that crystallization of mSPP may be possible with conditions used for MCMJRSPP. Other SPP/SPPL may crystallize under the same or similar conditions.

Further 2D crystallization trials are planned to answer pivotal questions about the structure and function of SPP, such as how do aspartyl proteases hydrolyze peptide bonds in a hydrophobic environment, how do aspartyl proteases determine which signal peptides and other membrane proteins to cleave, and finally how will a structure of an SPP homologue contribute to rational drug design.

REFERENCES

1. Krogh, A., Larsson, B., von Heijne, G. & Sonnhammer, E. L. (2001). Predicting transmembrane protein topology with a hidden Markov model: application to complete genomes. *J Mol Biol* 305(3): 567-580.

2. Alberts, B. (2002). Molecular Biology of the Cell. New York, Garland Science.

3. Yildirim, M. A., Goh, K., Cusick, M. E., Barabasi, A., & Vidal, M. (2007). Drug-target network. *Nat Biotechnol* 25(10): 1119-1126.

4. Overington, J. P., Al-Lazikani, B., & Hopkins, A. L. (2006). How many drug targets are there? *Nat Rev Drug Discov* 5(12): 993-996.

5. Fairman, J. W., Noinaj, N., & Buchanan, S. K. (2011). The structural biology of beta-barrel membrane proteins: a summary of recent reports. *Curr Opin Struct Biol* 21(4): 523-531.

6. Bordag, N & Keller, S. (2010). Alpha-helical transmembrane peptides: a Divide and Conquer approach to membrane proteins. *Chem Phys Lipids* 163:1-26.

7. Henderson, R. & Unwin, P. N. (1975). Three-dimensional model of purple membrane obtained by electron microscopy. *Nature* 257(5521): 28-32.

8. Ubarretxena-Belandia, I and Stokes, D. L. (2010). Present and future of membrane protein structure determination by electron crystallography. *Adv Protein Chem Struct Biol* 81:33-60.

9. Kühlbrandt, W. (2012). Combining Cryo-EM and X-ray Crystallography to Study Membrane Protein Structure and Function. Macromolecular Crystallography: Deciphering the Structure, Function and Dynamics of Biological Molecules. Ed. Maria Armenia Carronda and Paola Spadon. NATO Science for Peace and Security Series A: Chemistry and Biology. Springer, 2012, 93-101.

10. Oesterhelt, D. & Stoeckenius, W. (1971). Rhodopsin-like protein from the purple membrane of Halobacterium halobium. Nature New Biol 233: 149-152.

11. Walz, T. (1998). Electron crystallography of two-dimensional crystals of membrane proteins. *J Struct Biol* 121: 142-161.

12. Junge, F., Schneider, B., Reckel, S., Schwarz, D., Dotsch, V., & Bernhard, F. (2008). Large-scale production of functional membrane proteins. *Cell Mol Life Sci* 65(11): 1729-1755.

13. Vinothkumar, K. R., Edwards, P. C., & Strandfuss, J. (2013). Practical aspects in expression and purification of membrane proteins for structural analysis. *Methods Mol Biol* 955: 17-30.

14. Schmidt-Krey, I. (2007a). Electron crystallography of membrane proteins: two-dimensional crystallization and screening by electron microscopy. *Methods* 41(4): 417-426.

15. Dreaden, T. M., Metcalfe, M. G., Kim, L. Y., Johnson, M. C., Barry, B. A., & Schmidt-Krey, I. (2013). Screening for two-dimensional crystals by transmission electron microscopy of negatively stained samples. *Methods Mol Biol* 955: 73-101.

16. Johnson, M. C., Dreaden, T. M., Kim, L. Y., Rudolph, F., Barry, B. A., & Schmidt-Krey, I. (2013). Two-dimensional crystallization of membrane proteins by reconstitution through dialysis. *Methods Mol Biol* 955: 31-58.

17. Fujiyoshi, Y. (2013). Low dose techniques and cryo-electron microscopy. *Methods Mol Biol* 955: 103-118.

18. Avila-Sakar, A., Li, X., Zheng, S. Q., & Cheng, Y. (2013). Recording high-resolution images of two-dimensional crystals of membrane proteins. *Methods Mol Biol* 955: 129-152.

19. Arheit, M. (2013). Image processing of 2D crystal images. *Methods Mol Biol* 955: 171-194.

20. Erez, E., Fass, D., & Bibi, E. (2009). How intramembrane proteases bury hydrolytic reactions in the membrane. *Nature* 459(7245): 371-378.

21. Weihofen, A., Binns, K., Lemberg, M. K., Ashman, K., & Martoglio, B. (2002). Identification of signal peptide peptidase, a presenilin-type aspartic protease. *Science* 296(5576): 2215-2218.

22. Ponting, C. P., Hutton, M., Nyborg, A., Baker, M., Jansen, K., & Golde, T. E. (2002). Identification of a novel family of presenilin homologues. *Hum Mol Genet* 11(9): 1037-1044.

23. Grigorenko, A. P., Moliaka, Y. K., Korovaitseva, H. I., & Rogaev, E. (2002). Novel class of polytopic proteins with domains associated with putative protease activity. *Biochemistry* (Mosc) 67(7): 826-835.

24. Friedmann, E., Lemberg, M. K., Weihofen, A., Dev, K. K., Dengler, U., Rovelli, G., & Martoglio, B. (2004). Consensus analysis of signal peptide peptidase and homologous human aspartic proteases reveals opposite topology of catalytic domains compared with presenilins. *J Biol Chem* 279(49): 50790-50798.

25. Fluhrer, R., Grammer, G., Israel, L., Condron, M. M., Haffner, C., Friedmann, E., Böhland, C., Imhof, A., Martoglio, B., Teplow, D. B., & Haass, C. (2006). A gamma-secretase-like intramembrane cleavage of TNF alpha by the GxGD aspartyl protease SPPL2b. *Nat Cell Biol* 8(8): 894-896.

26. Friedmann, E., Hauben, E., Maylandt, K., Schleeger, S., Vreugde, S., Lichtenthaler, S. F., Kuhn, P.H., Stauffer, D., Rovelli, G., & Martoglio, B. (2006). SPPL2a and SPPL2b promote intramembrane proteolysis of TNF alpha in activated dendritic cells to trigger IL-12 production. *Nat Cell Biol* 8(8): 843-848.

27. Kirkin, V., Cahuzac, N., Guardiola-Serrano, F., Huault, S., Lückerath, K., Friedmann, E., Novac, N., Wels, W. S., Martoglio, B., Hueber, A.O., & Zörnig, M. (2007). The Fas ligand intracellular domain is released by ADAM10 and SPPL2a cleavage in T-cells. *Cell Death Differ* 14(9): 1678-1687.

28. Voss, M., Fukumori, A., Kuhn, P.H., Künzel, U., Klier, B., Grammer, G., Haug-Kröper, M., Kremmer, E., Lichtenthaler, S. F., Steiner, H., Schröder, B., Haass, C., & Fluhrer, R. (2012). Foamy virus envelope protein is a substrate for signal peptide peptidase-like 3 (SPPL3). *J Biol Chem* 287(52): 43401-43409.

29. Lemberg, M. K. & Martoglio, B. (2002). Requirements for signal peptide peptidase-catalyzed intramembrane proteolysis. *Mol Cell* 10(4): 735-744.

30. Nyborg, A. C., Kornilova, A. Y., Jansen, K., Ladd, T.B., Wolfe, M.S., & Golde, T. E. (2004). Signal peptide peptidase forms a homodimer that is labeled by an active site-directed gamma-secretase inhibitor. *J Biol Chem* 279(15): 15153-15160.

31. Miyashita, H., Maruyama, Y., Isshiki, H., Osawa, S., Ogura, T., Mio, K., Sato, C., Tomita, T., & Iwatsubo, T. (2011). Three-dimensional structure of the signal peptide peptidase. *J Biol Chem* 286(29): 26188-26197.

32. Li, X., Dang, S., Yan, C., Gong, X., Wang, J., & Shi, Y. (2013). Structure of a presenilin family intramembrane aspartate protease. *Nature* 493(7430): 56-61.

33. Voss, M., Schroder, B., & Fluhrer, R. (2013). Mechanism, specificity and physiology of signal peptide peptidase (SPP) and SPP-like proteases. *BBA* 1828: 2828-2839.

34. McLauchlan, J., Lemberg, M. K. Hope, G., & Martoglio, B. (2002). Intramembrane proteolysis promotes trafficking of hepatitis C virus core protein to lipid droplets. *EMBO* 21(15): 3980-3988.

35. Okamoto, K., Moriishi, K., Miyamura, T., & Matsuura, Y. (2004). Intramembrane proteolysis and endoplasmic reticulum retention of hepatitis C virus core protein. *J Virol* 78(12): 6370-6380.

36. Ait-Goughoulte, M., Hourioux, C., Patient, R., Trassard, S., Brand, D., & Roingeard, P. (2006). Core protein cleavage by signal peptide peptidase is required for hepatitis C virus-like particle assembly. *J Gen Virol* 87(Pt 4): 855-860.

37. Targett-Adams, P., Schaller, T., Hope, G., Lanford, R. E., Lemon, S. M., Martin, A., & McLauchlan, J. (2006). Signal peptide peptidase cleavage of GB virus B core protein is required for productive infection in vivo. *J Biol Chem* 281(39): 29221-29227.

38. Crawshaw, S. G., Martoglio, B., Meacock, S.L., & High, S. (2004). A misassembled transmembrane domain of a polytopic protein associates with signal peptide peptidase. *Biochem J* 384(Pt 1): 9-17.

39. Schrul, B., Kapp, K., Sinning, I., & Dobberstein, B. (2010). Signal peptide peptidase (SPP) assembles with substrates and misfolded membrane proteins into distinct oligomeric complexes. *Biochem J* 427(3): 523-534.

40. Lemberg, M. K., Bland, F. A., Weihofen, A., Braud, V. M., & Martoglio, B. (2001). Intramembrane proteolysis of signal peptides: an essential step in the generation of HLA-E epitopes. *J Immunol* 167(11): 6441-6446.

41. Martoglio, B., Graf, R., & Dobberstein, B. (1997). Signal peptide fragments of preprolactin and HIV p-gp160 with calmodulin. *EMBO* 16(22): 6636-6645.

42. Weihofen, A., Lemberg, M. K., Ploegh, H. L., Bogyo, M., & Martoglio, B. (2000). Release of signal peptide fragments into the cytosol requires cleavage in the transmembrane region by a protease activity that is specifically blocked by a novel cysteine protease inhibitor. *J Biol Chem* 275(40): 30951-30956.

43. Laudon, H., Hansson, E. M., Melén, K., Bergman, A., Farmery, M. R., Winblad, B., Lendahl, U., von Heijne, G., & Näslund, J. (2005). A nine-transmembrane domain topology for presenilin 1. *J Biol Chem* 280(42): 35352-35360.

44. Edbauer, D., Winkler, E., Regula, J. T., Pesold, B., Steiner, H., & Haass, C. (2003). Reconstitution of gamma-secretase activity. *Nat Cell Biol* 5(5): 486-488.

45. Harris, J. R. (1999). Negative staining of thinly spread biological particulates. *Methods Mol Biol* 117: 13-30.

46. Beebe, E. T., Makino, S., Nozawa, A., Matsubara, Y., Frederick, R.O., Primm, J. G., Goren, M. A., & Fox, B. G. (2011). Robotic large-scale application of wheat cell-free translation to structural studies including membrane proteins. *N Biotechnol* 28(3): 239-249.

47. Gipson, B., Zeng, X., Zhang, Z. Y., & Stahlberg, H. (2007). 2dx--user-friendly image processing for 2D crystals. *J Struct Biol* 157(1): 64-72.

48. Abeyrathne, P. D., Arheit, M., Kebbel, F., Castano-Diez, D., Goldie, K. N., Chami, M., & Stahlberg, H. (2012). Analysis of 2-D Crystals of Membrane Proteins by Electron Microscopy. *Comprehensive Biophysics* **1**, 277-310

49. Schmidt-Krey, I., Kanaoka, Y., Mills, D. J., Irikura, D., Haase, W., Lam, B. K., Austen, K. F., & Kühlbrandt, W. (2004). Human leukotriene C(4) synthase at 4.5 A resolution in projection. *Structure* 12(11): 2009-2014.

50. Schmidt-Krey, I., Haase, W., Mutucumarana, V., Stafford, D. W., & Kühlbrandt, W. (2007b). Two-dimensional crystallization of human vitamin K-dependent gamma-glutamyl carboxylase. *J Struct Biol* 157(2): 437-442.

51. Schmidt-Krey, I., Lundqvist, G., Morgenstern, R., & Hebert, H. (1998). Parameters for the two-dimensional crystallization of the membrane protein microsomal glutathione transferase. *J Struct Biol* 123(2): 87-96.

52. sbkb.org. (April 27, 2012). Structural Biology Center: Protocol ID: LP.909 (Oct. 22, 2012). from http://sbkb.org/tt/protocol?ttid=TEMIMPS-GO.15205&lab=TEMIMPS&trialid=2&protocolid=LP.909

53. Vink, M., Derr, K., Love, J., Stokes, D. L., & Ubarretxena-Belandia, I. (2007). A high-throughput strategy to screen 2D crystallization trials of membrane proteins. *J Struct Biol* 160(3): 295-304.

54. Kebbel, F., Kurz, M., Grütter, M. G., & Stahlberg, H. (2012). Projection structure of the secondary citrate/sodium symporter CitS at 6 A resolution by electron crystallography. *J Mol Biol* 418(1-2): 117-126.

55. Kebbel, F., Kurz, M., Arheit, M., Grütter, M. G., & Stahlberg, H. (2013). Structure and substrate-induced conformational changes of the secondary citrate/sodium symporter CitS revealed by electron crystallography. *Structure* 21(7): 1243-1250.